CHEMISTRY

Microenvironment modulation of single-atom catalysts and their roles in electrochemical energy conversion

Xuning Li[1], Linghui Liu[2], Xinyi Ren[2], Jiajian Gao[1], Yanqiang Huang[2]*, Bin Liu[1]*

Single-atom catalysts (SACs) have become the most attractive frontier research field in heterogeneous catalysis. Since the atomically dispersed metal atoms are commonly stabilized by ionic/covalent interactions with neighboring atoms, the geometric and electronic structures of SACs depend greatly on their microenvironment, which, in turn, determine the performances in catalytic processes. In this review, we will focus on the recently developed strategies of SAC synthesis, with attention on the microenvironment modulation of single-atom active sites of SACs. Furthermore, experimental and computational advances in understanding such microenvironment in association to the catalytic activity and mechanisms are summarized and exemplified in the electrochemical applications, including the water electrolysis and O_2/CO_2/N_2 reduction reactions. Last, by highlighting the prospects and challenges for microenvironment engineering of SACs, we wish to shed some light on the further development of SACs for electrochemical energy conversion.

INTRODUCTION

Renewable energy conversion and storage devices are critical in the effort to address the global energy consumption and environmental challenges (*1*, *2*). Electrochemical reactions, including the oxygen reduction reaction (ORR), hydrogen evolution reaction (HER), oxygen evolution reaction (OER), nitrogen reduction reaction (NRR), and carbon dioxide reduction reaction (CO_2RR), play key roles in sustainable energy conversion, storage, and utilization (*3*–*8*). The noble metals are currently the most frequently used catalysts to drive these reactions; however, the high cost and scarcity of these metals hinder the widespread adoption of these technologies (*9*–*11*). Therefore, it is highly desired but still challenging for developing alternative electrocatalysts with earth-abundant metals or reduced loading of precious metals. Furthermore, since the overall electrochemical performance of these reactions is highly sensitive to both the physical and chemical properties of the catalysts, the understanding of the structure-activity relationship of the reactive sites and the underlying reaction mechanism is substantial for the further development of efficient electrocatalysts.

Single-atom catalysts (SACs), with atomically distributed metal centers and maximized atom utilization efficiency, have attracted great attention in catalysis owing to the integrated merits of homogeneous and heterogeneous catalysts (*12*–*17*). The distinct atomic microenvironment (defined as a small, specific, and isolated chemicophysical environment, such as the local coordination environment and electronic state of the catalytic center) of SACs offers remarkable advantages to achieve high activity, selectivity, and stability for heterogeneous catalysis (*18*–*22*) and electrochemical applications (*23*–*28*). Previously, we have thoroughly summarized the advances of supported noble metal SACs for heterogeneous catalysis (*15*); however, few reports specified and highlighted the microenvironment engineering of SACs for electrochemical applications. Recently, diverse strategies have been developed for rational design of SACs with well-controlled microenvironments, and numbers of experimental and theoretical efforts have been made aimed at in-depth understanding of the microenvironment-activity relationships and the underlying reaction mechanisms in various electrochemical energy conversion reactions (*29*–*37*).

In this review, we aim to provide an overview toward the rational design of the microenvironments of SACs for electrochemical energy conversion applications. The recently developed synthetic strategies are thoroughly summarized. The notable breakthroughs that SACs have brought in various electrochemical reactions including OER, HER, ORR, CO_2RR, and NRR are highlighted. In particular, we discuss how different functionalities of SACs can be realized through the rational design and synthesis. Recent experimental and computational achievements in understanding the microenvironment-activity relationships and the associated mechanisms are summarized. In addition, the challenges and future directions for designing SACs with desired electrocatalytic performances for the potential practical energy conversion applications are discussed.

STRATEGIES FOR ALTERING THE MICROENVIRONMENTS OF SACs

The microenvironments of single-atom centers, such as geometric construction, coordination, and electronic structure, are extremely critical in optimizing the physical and chemical properties of SACs. Therefore, fabricating SACs with desired microenvironments while maintaining atomic dispersion of metal species is highly attractive and important. Recently, many synthetic strategies including defect engineering, metal-support interaction (MSI), heteroatom tethering, spatial confinement, atomic alloying, molecular bridging, etc. have been developed for the preparation of SACs with various microenvironments. Besides, metal-organic frameworks, owing to the well-defined structure and flexible adjustability, have attracted great attention in regulating the microenvironments of SACs.

Defect engineering

Controlled construction of surface defects on supports, which serve as "traps" to capture the metal atoms, has been proven effective for developing SACs with a well-defined microenvironment. Typically,

[1]School of Chemical and Biomedical Engineering, Nanyang Technological University, 62 Nanyang Drive, Singapore 637459, Singapore. [2]State Key Laboratory of Catalysis, Dalian Institute of Chemical Physics, Chinese Academy of Sciences, Dalian 116023, China.
*Corresponding author. Email: yqhuang@dicp.ac.cn (Y.H.); liubin@ntu.edu.sg (B.L.)

defects such as metal cation, oxygen, sulfur, and carbon vacancies, depending on the types of supports, are the most common sites for altering the microenvironments of single-atom sites.

For the single atoms anchored on metal oxide, cationic vacancies have been widely exploited for developing SACs with well-defined local environments (*16*–*46*). For instance, single Pt_1 atoms coordinated by three dangling oxygen atoms supported on hematite could be successfully achieved through the surface Fe vacancies (*16*). Isolated Pt species with a range of oxidation states and local coordination environments could be hosted by Ti vacancies on anatase TiO_2 surface (*46*). In Pt_1/CeO_2 SACs, single Pt atoms with a PtO_4 core stabilized in Ce vacancies on CeO_2 surface was evidenced by density functional theory (DFT) calculations (Fig. 1A) (*38*). Recently, in the work conducted by Wang and colleagues (*47*), by electrochemical exfoliation, abundant exposed Mo vacancies in the outer layers of double transition metal MXenes ($Mo_2TiC_2T_x$) were created and used to immobilize positively charged Pt single atoms through covalent bonding. Defects of surface oxygen vacancies have also been proved as ideal sites to anchor single metal atoms (*39*, *48*, *49*). As shown in Fig. 1B, by constructing oxygen vacancies on the surface of TiO_2, single Au atoms supported on defective TiO_2 nanosheets ($Au_1/Def\text{-}TiO_2$) with the formation of Ti-Au-Ti structure could be obtained (*39*). In the work conducted by Li and co-workers (*40*), Cu atom-pair catalyst (APC) was developed by constructing surface Te defects on $Pd_{10}Te_3$ alloy nanowires (Fig. 1C). With the optimal Cu loading ratio of 0.10 weight % (wt %), a stable Cu_1^0-Cu_1^{x+} atom-pair structure was created and identified.

The important role of sulfur vacancies for trapping single metal atoms has also been revealed in layered transition metal dichalcogenide (MoS_2 and WS_2) as support (*41*, *42*). For instance, as shown in Fig. 1D, a high-angle annular dark-field scanning transmission electron microscopy (HAADF-STEM) image and the DFT relaxed atomic model of Pt_1/MoS_2 clearly illustrate that the single Pt atoms are hosted in a 2S vacancy (*41*). In addition, isolated Co atoms coordinated covalently to sulfur vacancies on MoS_2 monolayer sheets (Co_1/MoS_2 SAC) was synthesized by Tsang and colleagues through Li intercalation and chemical exfoliation (*42*). Experiments and DFT calculations reveal that abundant Co-S-Mo interfacial sites were created local to the sulfur vacancies (Fig. 1E), which was ascribed as the main factor for the superior catalytic performance.

Carbon vacancy is also a common type of defect, which can provide efficient anchoring sites for stabilizing single metal atoms via the strong charge transfer between the *2p* antibonding state of the carbon atoms and the metal atoms (*30*, *50*). Defective graphene (DG) matrices, with or without doped heteroatoms as anchoring sites, have attracted great interest as hosts for single atoms owing to their chemical stability and high electron conductivity (*24*). For instance, via a versatile gas-transport strategy, the sublimated mobile Cu atoms from copper (I) oxide powder at nearly melting temperature could be trapped by defect-rich nitrogen-doped carbon (NC), forming the isolated single-atom copper site (Cu ISAS/NC) catalyst (*51*). The thermal emitting method was also used by Wu and co-workers to generate atomically dispersed platinum on DG (Pt SAs/DG) (*52*). Recently, a facile strategy using an impregnation method was developed by Yao and co-workers for fabricating a highly stable single–Ni atom catalyst on DG (*43*). Through DFT calculations, several stable Ni-C coordination structures (Fig. 1F) were identified and further confirmed in HAADF-STEM images (Fig. 1G). The results from these works provide approaches for developing SACs with controlled microenvironments through defect engineering strategy.

Metal-support interaction

Besides the diverse defective sites for stabilizing isolated atoms in SACs, MSI is proposed to modulate the electronic structure of single atoms through the covalent/ionic chemical bonding effect with supports (*44*). For instance, Qiao and co-workers reported the formation of single Pt atoms on Fe_2O_3 during methane oxidation through a strong covalent MSI with iron and oxygen atoms, which is not associated with support defects (Fig. 1H) (*44*). Experimental and DFT studies reveal that the reducibility of iron oxide is crucial for trapping isolated Pt atoms. Recently, a facile dangling bond trapping strategy was developed by Wu and co-workers to construct SACs on graphene oxide (M SAs/GO; M = Fe, Co, Ni, and Cu) (*45*). The abundant oxygen-containing functional groups on GO have been shown as the main sites to grab the metal atoms (Fig. 1I). In addition, the charge transfer from M^0 to the dangling oxygen groups resulted in the isolated $M^{\delta+}$ ($0 < \delta < 3$) species with the formation of M—O bonds. Despite the recent achievements, more strategies for the precise control of electronic and coordination environment of SACs are highly desired.

Heteroatom tethering

Heteroatom tethering, which provides anchoring sites for fixing metal atoms through MSI, has also attracted great research interests. In carbon-based supports, control over the content of heteroatom such as N, P, S, O, or B provides immense scope for tuning the microenvironments of the single-atom sites within the functionalized carbons (*23*, *31*, *53*–*55*). For instance, Liang and co-workers developed a sulfur-tethering strategy for the synthesis of noble metal SACs with high metal loading up to 10 wt % (*33*), and the results indicate that the doping of sulfur endows mesoporous carbon with high-density anchoring sites for bonding metal atoms via the strong metal-sulfur interactions. By using porous N,S–co-doped carbon (NSC) matrix as host, Fe-SAs/NSC with well-dispersed FeN_4S_2 sites could be synthesized (*56*). In addition, the doping of S atoms in Ni-SAs/NSC and Co-SAs/NSC enabled the formation of NiN_3S_1 and CoN_3S_1 sites. All these recent advances clearly demonstrate the feasibility for altering the microenvironments of SACs via MSI; however, besides the carbon-based materials, more studies on many other supports such as metal oxides and polyoxometalates may expand a wider world for the development of SACs.

Spatial confinement

Spatial confinement has been developed as an effective approach to construct SACs with well-defined microenvironments. For the spatial confinement strategy, both selection of supports having uniform pore structures and mononuclear metal precursors with suitable charge state and molecular size are of great significance for altering the microenvironments of single-atom sites. Porous materials including zeolites, covalent-organic frameworks, metal–organic frameworks (MOFs), porous carbon matrix (PCM), etc. have been considered as ideal hosts for encapsulating mononuclear metal precursors. Owing to the microporous diffusion limitation, the spatial confinement strategy ensures uniform dispersion of the precursors. Followed by a posttreatment to remove ligands of precursors, SACs with uniform single metal atoms stabilized by the skeletons of supports could be achieved. For instance, by in situ confining and

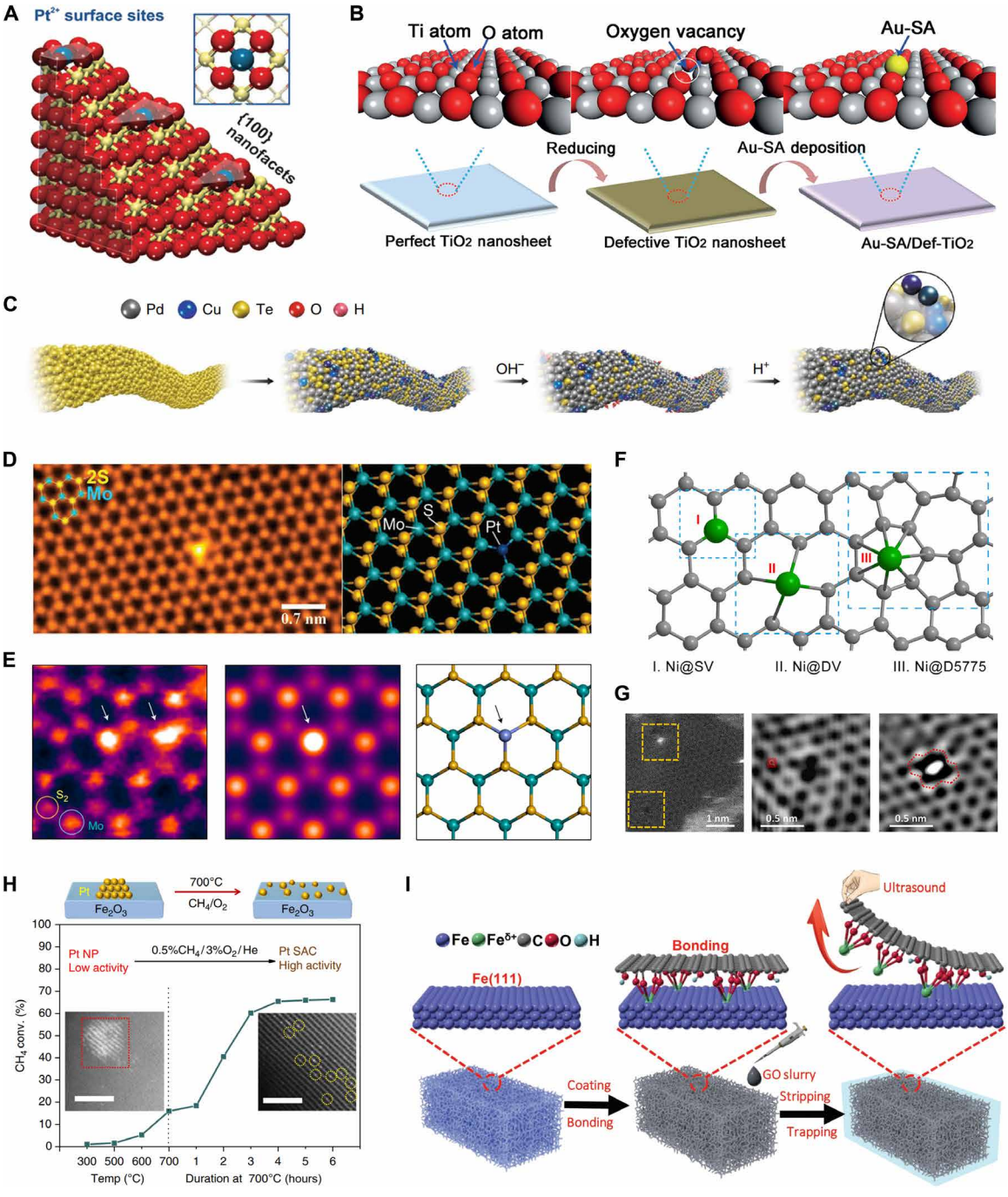

Fig. 1. Defect and MSI strategy for the synthesis of SACs. (**A**) DFT atomic model of Pt_1/CeO_2 illustrating single Pt atoms with a PtO_4 core anchored on CeO_2, adapted with permission from Bruix *et al*. (*38*). (**B**) Schematic illustration for the synthesis of Au_1/Def-TiO_2, adapted with permission from Wan *et al*. (*39*). (**C**) Schematic illustration for the synthesis of Cu atom pair anchored on $Pd_{10}Te_3$ nanowires, adapted with permission from Jiao *et al*. (*40*). (**D**) High-angle annular dark-field scanning transmission electron microscopy (HAADF-STEM) image and DFT relaxed atomic model of Pt_1/MoS_2 illustrating a Pt atom in a 2S vacancy, adapted with permission from Li *et al*. (*41*). (**E**) HAADF-STEM image, simulated HAADF-STEM image, and atomic model of Co_1/MoS_2, adapted with permission from Liu *et al*. (*42*). (**F**) Schematic of Ni atoms (green balls) stabilized in single-vacancy (SV), double-vacancy (DV), and 5775 (D5775) carbon defects, adapted with permission from Jiang and Wang (*30*). (**G**) HAADF-STEM images of graphene defects with or without a trapped Ni atom, adapted with permission from Zhang *et al*. (*43*). (**H**) Dynamic formation of single Pt atoms on Fe_2O_3 during methane oxidation through a strong covalent interaction with oxygen and iron atoms, adapted with permission from Lang *et al*. (*44*). (**I**) Schematic illustration for the stabilization of single Fe atoms coordinated by the surface oxygen dangling bonds on graphene oxide (GO), adapted with permission from Qu *et al*. (*45*).

separating a metal-ethylenediamine (M = Pt, Pd, Ru, Rh, Co, Ni, and Cu) complex into the β-cages of Y zeolite during crystallization followed by a thermal treatment process, a series of isolated single metal atomic site catalysts (M-ISAS@Y) were synthesized (*57*). In the work conducted by Lou and colleagues (*58*), a dynamic reaction strategy to stabilize single Pt atoms in PCM (Pt@PCM) was developed. As shown in Fig. 2A, the dynamic reaction through electrostatic interaction led to the traction and relocation of the single Pt atoms from the surface into the interior of the carbon matrix, which were then converted into Pt@PCM via a stepwise pyrolysis process. Recently, via directly loading Fe species on SBA-15 and a subsequent thermal treatment process (Fig. 2B), Sun and co-workers demonstrated the generation of an SBA-15 confined single–Fe atom catalyst (*59*). Extended x-ray absorption fine structure (EXAFS) fitting results confirm the presence of atomically dispersed O-Fe sites with an average coordination number of 4.5. In the work performed by Zhang *et al.* (*60*), single–Pt atom catalysts were constructed using hierarchical NC nanocages as host. Theoretical simulation revealed that the isolated platinum atoms were confined in the micropores with edge-nitrogen dopants by trapping and anchoring $[PtCl_6]^{2-}$ species (Fig. 2C). All these results suggest the versatility of the spatial confinement strategy in designing the local coordination environment of SACs.

Atomic alloying

Atomic alloying offers a useful route to tune the bonding geometry and electronic structure of the single-metal sites in single-atom alloys (SAAs) that are composed of one type of metal atoms isolated in an array of atoms of a second metal. Recently, Zhang and co-workers developed a facile colloidal method to synthesize bimetallic Pt-Au SAA and nanoparticle (Fig. 2D) (*26*). Experimental and theoretical studies evidenced the surface single–Pt atom sites surrounded by Au atoms in Pt_4Au_{96} and Pt_7Au_{93} SAAs and the unique alloy-bonding properties and structure of these single–Pt atom species for the superior catalytic performance. Theoretical predictions carried out by Greiner *et al.* (*25*) show the free atom-like electronic structure on the single metal atoms in SAA. As shown in Fig. 2E, the charge-density difference plots clearly indicate the increase of charge density around the Cu ion, behaving like a free atom. The bonding of adsorbates to single metal atoms in SAA resembles the bonding in molecular metal complexes owing to the unusual electronic structure, resulting in unprecedented catalytic properties. Therefore, atomic alloying offers a powerful design strategy to alter the electronic structure of single–metal atom sites.

Molecular bridging

Molecular bridging including covalent or noncovalent (π stacking, hydrophobic, etc.) approaches has recently been demonstrated as a general method for introducing well-defined single-atom sites on conducting materials. Owing to the high electrical conductivity and surface area, carbon nanotubes and graphene have attracted great interest for this purpose (*61*–*63*). For instance, by using the molecular bridging method, a covalent network of cobalt-porphyrin with well-defined CoN_4 center on multiwalled carbon nanotube (MWNT) surface (MWNT-CoP) was synthesized by Hijazi *et al.* (*64*). As shown in Fig. 2F, coupling of CoP on a MWNT surface provides a robust method for the functionalization of carbon nanotubes with well-defined single-atom species through multiple π-π interactions. In the work conducted by Peng *et al.* (*65*), a pyrolysis-free synthetic approach was developed to prepare SACs with atomically well-designed Fe-N-C centers. The fully π-conjugated iron phthalocyanine (FePc) was grafted on the graphene matrix via the intermolecular interactions. Recently, Liu *et al.* constructed a model single–Ni atom catalyst (Ni SAC) with precise structure via a two-step molecular bridging approach (Fig. 2G). Results from the aberration-corrected HAADF-STEM and x-ray absorption spectroscopy (XAS) measurements clearly confirm the well-defined Ni-N_4 moiety on carbon support (*66*).

Catalysts with atomically dispersed diatomic clusters could also be developed through the preselected metal precursors. For instance, Li and co-workers recently reported the synthesis of a mesoporous carbon nitride (mpg-C_3N_4)–supported Fe_2 cluster catalysts through a "precursor-preselected" wet-chemistry strategy, which could also be applied for producing other diatomic clusters such as Ir_2 and Pd_2 anchored on mpg-C_3N_4 (*67*).

For molecular bridging approaches, the covalent grafting of molecules on carbon materials usually produces robust assemblies; however, the transformation of sp^2 hybridized carbon atoms to sp^3 leads to the loss of their electronic properties. In contrast, the noncovalent approach can maintain the electronic properties of carbon materials but results in poor stability because of the weak interactions. Therefore, the development of novel techniques that balance both the electronic properties and stability of the atomically dispersed molecular sites is still very challenging.

Mof derivatization

MOFs have become the most promising precursors for the construction of SACs over the past few years (*29*, *68*). Owing to the well-defined pore structures and highly ordered arrangements of the metal nodes and organic linkers, atomically dispersed metal sites can be flexibly introduced in pristine MOFs, followed by a thermal or chemical conversion process; SACs with well-controlled microenvironment could be obtained.

Now, a large variety of MOFs have been developed as promising platforms to prepare SACs. For instance, by using the strong coordination between the Ru atoms and free amine groups at the skeleton of derivative MOFs (UiO-66-NH_2), a precise control of a single–Ru atom site on nitrogen-doped porous carbon (Ru SAs/N-C) was realized by Li and co-workers (*69*). As shown in Fig. 2H, the abundant dangling -NH_2 groups in UiO-66-NH_2 benefit the adsorption of Ru metal ions in the MOF channels via the coordination interaction between the d orbital of Ru atoms and the lone electron pair of nitrogen, which could be further converted to Ru SAs/N-C with abundant single Ru sites coordinated to single-mind N. In the work conducted by Liu and colleagues (*70*), by pyrolyzing Fe-Co Prussian blue analog (PBA) followed by an acid treatment step, porous N-doped graphene confined single cobalt atoms with CoN_4 coordination configuration could be obtained (Fig. 2I).

Besides, more researches are still focusing on ZIF-8, which is constructed with 2-methylimidazolate as the organic linker and Zn cation as the metal node. During pyrolysis at temperatures higher than 900°C, Zn could be evaporated away while M-imidazolate-M linkages (M = Fe, Co, Ni, Cu, etc.) would be converted to M—N bonds. SACs with diverse coordination configurations are possible to be prepared through modulation of the organic linkers, metal nodes, and thermal or chemical treatment conditions. For instance, by simply changing the calcination temperature, Li and co-workers realized the flexible regulation of the N coordination number of atomically dispersed Co species. As

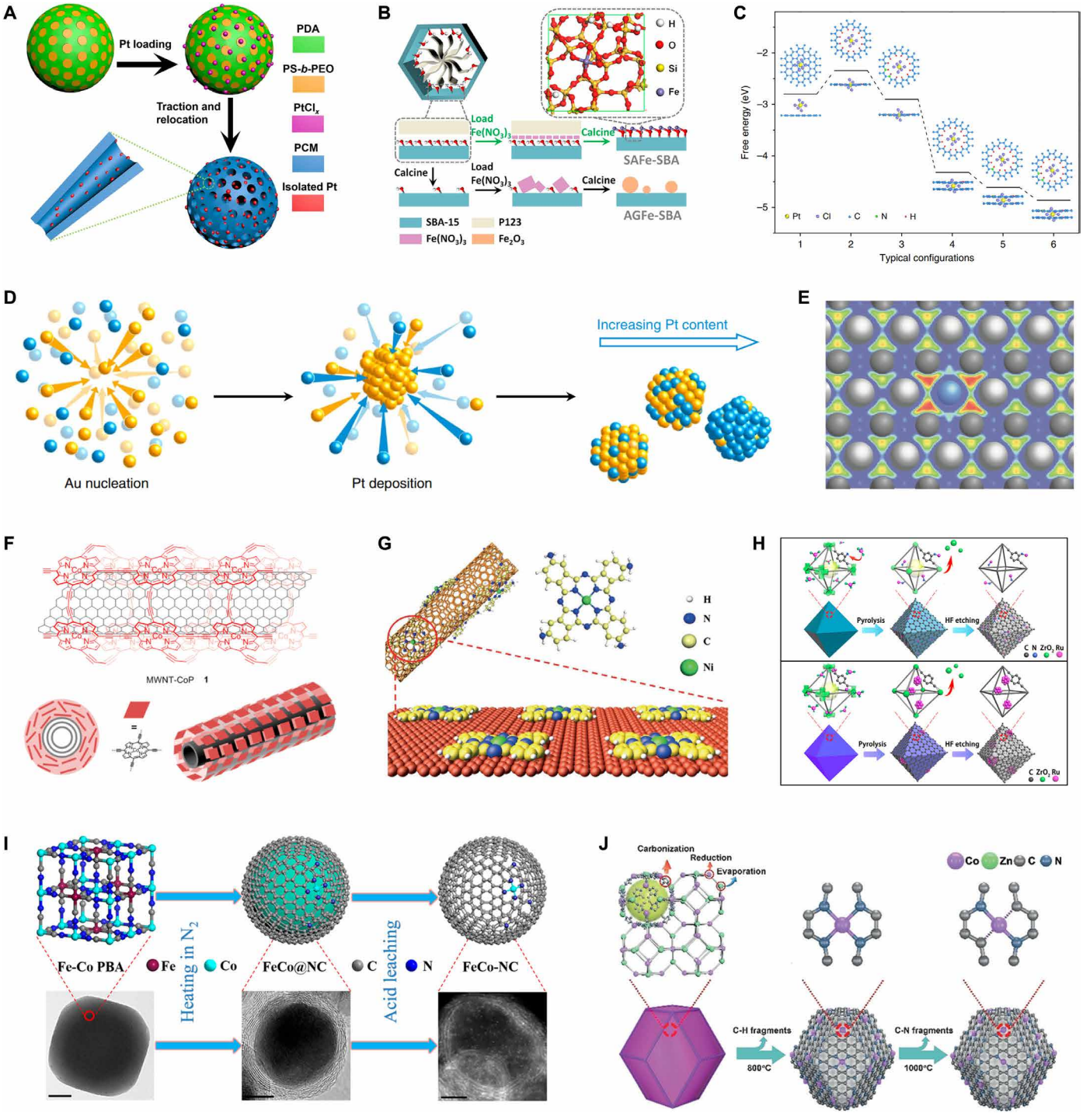

Fig. 2. Spatial confinement, atomic alloying, molecular bridging, and MOF derivatization strategies for the synthesis of SACs. (**A**) Schematic illustration of the confinement of isolated Pt atoms in PCM (Pt@PCM), adapted with permission from Zhang *et al*. (*58*). PDA, polydopamine; PEO, poly(ethylene oxide). (**B**) Illustration of the decoration of single–Fe atom sites on SBA-15, adapted with permission from Yin *et al*. (*59*). (**C**) Typical configurations of the micropore confined isolated $[PtCl_6]^{2-}$ species together with calculated free energies, adapted with permission from Zhang *et al*. (*60*). (**D**) Illustration for the formation of bimetallic Pt-Au single-atom alloy (SAA) and nanoparticle, adapted with permission from Duchesne *et al*. (*26*). (**E**) Calculated charge density difference along the (110) plane in $Ag_{31}Cu_1$ SAA, adapted with permission from Greiner *et al*. (*25*). (**F**) Scheme for the synthesis of covalent porphyrin network around multiwalled carbon nanotube (MWNT) surfaces, adapted with permission from Hijazi *et al*. (*64*). (**G**) Synthesis of model Ni SACs on carbon nanotubes, adapted with permission from Liu *et al*. (*66*). (**H**) Scheme for the formation of Ru SAs/N-C and Ru NCs/C, adapted with permission from Wang *et al*. (*69*). HF, hydrofluoric acid. (**I**) Preparation route and model of single–Co atom catalyst from Prussian blue analog (PBA), adapted with permission from Li *et al*. (*70*). (**J**) The formation process of Co-N_4 and Co-N, adapted with permission from Wang *et al*. (*71*).

shown in Fig. 2J, CoN_4, CoN_3, and CoN_2 with different Co-N numbers were obtained at the calcination temperature of 800°, 900°, and 1000°C, respectively (*71*). Moreover, by introducing multiple types of metal atoms to replace a certain proportion of Zn, atomically dispersed dual-metal sites anchored on NC such as Fe-Co, Fe-Ni dual-atom catalysts could also be developed using this strategy (*72*–*74*). The recent advances clearly show the bright prospects for rational design of SACs by integrating the advantages of diverse MOFs.

All these recent advances have clearly demonstrated that the versatile strategies including defect engineering, heteroatom tethering, spatial confinement, atomic alloying, molecular bridging, MOF derivatization, etc. are powerful in altering the microenvironments of SACs. Among them, molecular bridging is shown to be a promising method for designing "model SACs" by introducing well-defined single-atom sites on conducting materials. However, most of these strategies can only realize the "average control" of the geometric and electronic structures of single-atom sites. Further development for the "precise control" of the microenvironments in SACs is still challenging but highly desired.

CHARACTERIZATION OF SACs

Now, many advanced characterization techniques including aberration-corrected HAADF-STEM, XAS, Mössbauer spectroscopy, nuclear resonance vibrational spectroscopy, etc. have been widely used for identifying the precise microenvironment of SACs. Moreover, various in situ/operando characterization techniques have been developed for capturing the reaction intermediates and monitoring the dynamic behaviors of the microenvironment of the catalytic centers. The integrated application of these advanced techniques provides valuable opportunities for designing highly active SACs toward potential practical applications, which has been thoroughly summarized in our recent perspective (*75*).

ELECTROCHEMICAL APPLICATIONS OF SACs

The atomically dispersed metal atoms with well-defined microenvironments on supports enable SACs as promising advanced materials for various electrochemical energy conversion applications. Through the rational design of microenvironments of single-atom sites, SACs can achieve distinguished activity, stability, and selectivity for a wide variety of electrochemical reactions such as ORR, HER, OER, NRR, and CO_2RR. Below, we will highlight the recent breakthroughs of SACs in these electrochemical reactions. In particular, recent experimental and computational studies on understanding the microenvironment-activity relationships and the catalytic mechanisms will be discussed.

Oxygen reduction reaction

ORR occurring at the cathode is a key reaction in the development of fuel cells and metal-air batteries for green energy conversion. However, due to the sluggish kinetics of ORR, developing efficient catalysts with minimal content of precious metal and high performance is highly demanded.

The ORR follows either a two-electron ($2e^-$) or four-electron ($4e^-$) pathway, desirable for H_2O_2 production or fuel cell, respectively, which has been found to depend mainly on the microenvironments of SACs. For instance, the S-coordinated single–Pt atom site (PtS_4) was determined to catalyze the ORR via the $2e^-$ pathway (*76*), while C-coordinated and N-coordinated single–Pt atom sites preferred the $4e^-$ reaction pathway (*77*–*79*). In the work conducted by Li *et al.* (*79*), Pt_1/α-MoC and Pt_1/MoN SACs, with atomically dispersed Pt atoms anchored on α-MoC and MoN, respectively, were synthesized to study the effect of coordination environment of Pt atoms for ORR. As shown in Fig. 3A, the Pt atoms were demonstrated to be coordinated with Mo atoms in the Pt_1/α-MoC but with N atoms in the Pt_1/MoN. Compared to Pt_1/α-MoC, the weaker adsorption of OH* for Pt_1/MoN resulting from the modified electronic properties of Pt coordinated with N atoms was determined critical for the high ORR catalytic performance. Liu *et al.* reported the carbon defect–anchored Pt SACs (Pt_1/C) with remarkable ORR performance. DFT calculations indicate that the single Pt atoms coordinated by four carbon atoms in carbon divacancies (Fig. 3B), with optimized adsorption energy for the rate-controlling OH* intermediates, are the main active sites for realizing the excellent ORR performance (*78*).

Heteroatom coordinated M-N-C SACs (M = Fe, Co, Mn, Cu, etc.) are promising alternatives to Pt-based ORR catalysts (*65*, *80*–*86*). The intrinsic activity and ORR reaction pathway catalyzed by M-N-C SACs highly depend on the geometrical and electronic environment of the single-atom metal centers. For instance, a wide range tuning of $2e^-/4e^-$ ORR pathways was achieved in the work conducted by Wang and colleagues (*87*) via modulating the metal centers or neighboring metalloid coordination of SACs. The single Fe atoms in Fe-C-O species, which generally strengthen the binding of *OOH on C sites, were identified as highly active and selective for the H_2O_2 production via the $2e^-$ pathway. Recently, Liu and co-workers developed a kinetic model that constructs a quantitative relation between the electrochemical kinetic fingerprints and energy profile of oxygen redox (*88*). As shown in Fig. 3C, Fe-N-C has the optimal binding energy in alkaline media, resulting in the optimum ORR performance near the top of the volcano plot. As a typical Lewis base site, the coordination of N atom can withdraw electrons from single-atom metal sites, which plays a key role in weakening the rate-limited OOH* or OH* bonding energy and, thus, enhancing ORR activity.

In the work conducted by Yang *et al.* (*89*), the difference between Gibbs free energies for four-electron and two-electron transfer ORR (ΔG_{H2O}-ΔG_{H2O2}) of Fe@pyridinic N, Fe@pyrrolic N, and Pt(111) was found to be consistent with the production of H_2O_2 (Fig. 3D), indicating the Fe-pyrrolic-N species as the main active sites for ORR. However, the Fe-pyridinic-N moieties experience difficulty in adsorbing reaction intermediates because of a lower energy level location of the p band compared to that of Fe-pyrrolic-N moieties. The ORR performance catalyzed by M-N-C could be improved through S doping, which reduced the energy barriers of the reaction intermediates owing to the coordination of S atom (*56*, *90*). For instance, Zhu and co-workers demonstrated that the ORR activity of Fe-N-C could be improved with optimizing the charge and spin distributions of Fe via S doping (*90*). Further study conducted by Zhang *et al.* (*56*) suggests that the S-coordinated Fe atom sites play a vital role in lowering the reaction barrier (Fig. 3E), which is due to the modified Fe d orbitals with the highest occupied states near the Fermi level, boosting the ORR kinetics. Rational tailoring of Fe-N coordination number provides another way to enhance the ORR activity (*91*). For instance, in the work done by Zhu *et al.* (*91*, *92*), the Fe-N-C catalyst with FeN_2 active site was found with superior ORR activity owing to the high affinity to O_2 and low energy

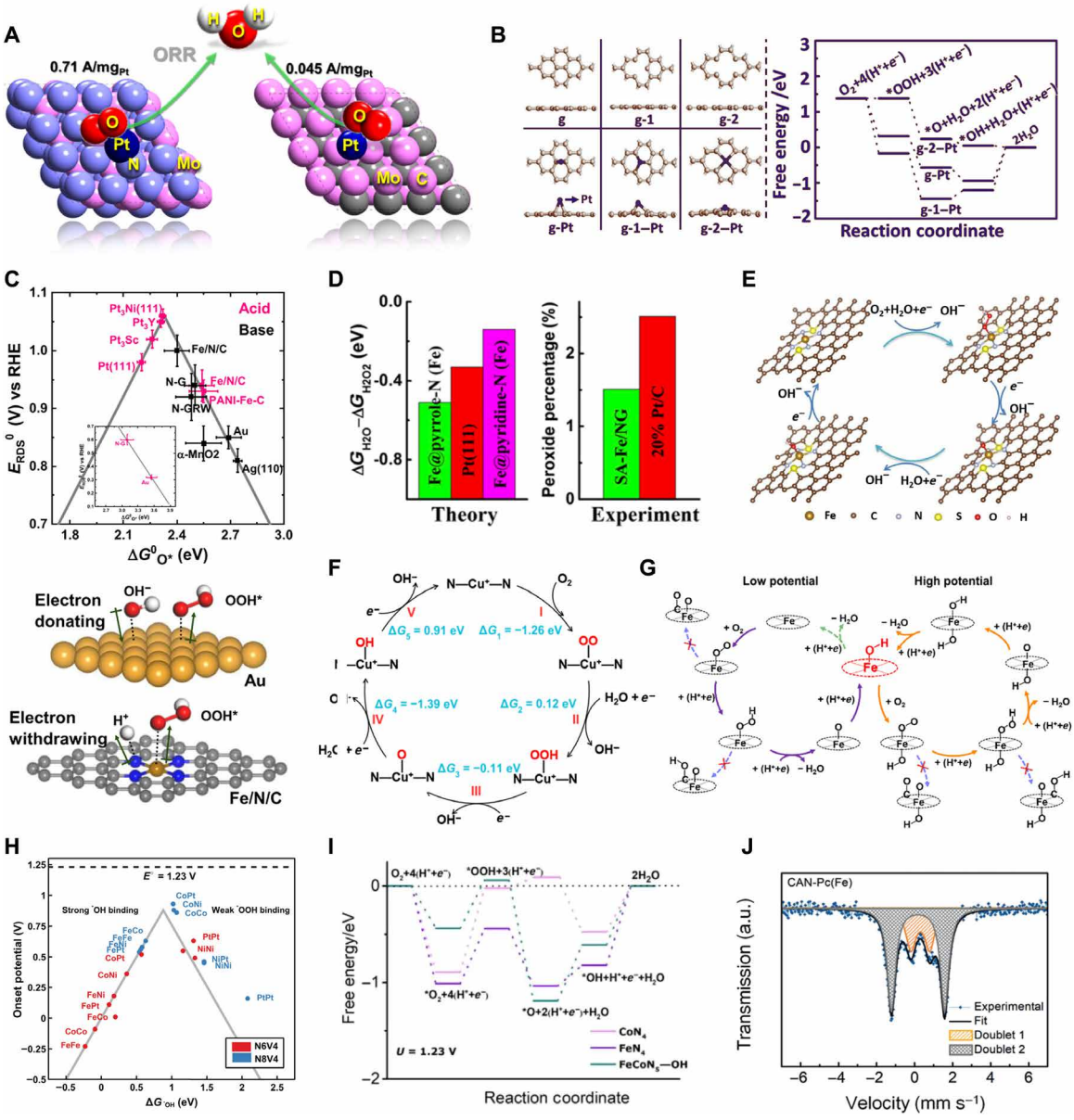

Fig. 3. Applications of SACs in ORR. (**A**) Single–Pt atom catalysts supported on α-MoC and MoN for ORR, adapted with permission from Li *et al*. (*79*). (**B**) Optimized structures of single Pt atom anchored on pristine graphene (g), monovacancy graphene (g-1), and divacancy graphene (g-2), together with the associated free energy diagram for ORR, adapted with permission from Liu *et al*. (*78*). (**C**) Activity volcano plot for ORR and the proposed mechanism, adapted with permission from Tao *et al*. (*88*). (**D**) The difference between Gibbs free energy for two-electron and four-electron transfer ORR ($\Delta G_{H2O} - \Delta G_{H2O2}$) at the potential determining step and the experimental peroxide percentage on different catalysts at U_{RHE} = 0.6 V, adapted with permission from Yang *et al*. (*89*). (**E**) Proposed ORR scheme on Fe-SAs/NSC, adapted with permission from Zhang *et al*. (*56*). (**F**) Proposed ORR mechanism on the Cu-N_2 single-atom site, adapted with permission from Wang *et al*. (*92*). (**G**) Proposed ORR mechanism on Fe-N-C SACs, adapted with permission from Wang *et al*. (*94*). (**H**) Activity volcano plot for ORR of different metal atoms (M = Co, Pt, Fe, and Ni) anchored in the pores of N_6V_4 and N_8V_4, adapted with permission from Hunter *et al*. (*95*). (**I**) Gibbs free energy diagrams on CoN_4, FeN_4, and $FeCoN_5$-OH sites, adapted with permission from Xiao *et al*. (*96*). (**J**) ^{57}Fe Mössbauer spectra of conjugated aromatic network involving transition metal phthalocyanines (CAN-FePc), adapted with permission from Yang *et al*. (*98*). a.u., arbitrary unit.

barriers for the intermediates and products. In addition, experimental and theoretical results from the work of Wang *et al*. (*92*) indicate that the unsaturated Cu^I-N_2 in Cu-N-C SAC acts as the active site for ORR via a $4e^-$ pathway (Fig. 3F). Recently, DFT studies carried out by Zhao *et al*. (*93*) suggest that the modification of single–metal atom centers with hydroxyl groups can largely improve the ORR activity of SACs. Furthermore, a self-adjusting mechanism proposed by Wang *et al*. (*94*) suggests that the single-atom Fe site in Fe-SAC was intrinsically covered with OH* intermediate existing as $Fe(OH)N_4$ species (Fig. 3G), which can optimize the electronic structure of single Fe atoms and boost the ORR. The construction of dual-metal sites in SACs has been shown with synergistic effects in improving the ORR performance. Recently, DFT studies performed by Hunter *et al*. (*95*) demonstrate that the spectating metal

partner in paired SACs can change the reduction potential of the atomically distributed metal atoms. As a result, paired Co and Pt atoms anchored on a N-doped four-atom vacancy graphene (N_8V_4) have been proposed as the best-performing system for ORR (Fig. 3H). In the work conducted by Xiao *et al.* (*96*), a OH-ligand self-binding strategy was proposed for ORR with Fe-Co dual-atom active sites for anchoring OH. The anchoring of OH on the triangle $FeCoN_5$ produced the $FeCoN_5$-OH site with optimal geometry configuration and e_g orbital energy level of Fe, thus enabling easier intermediate desorption and O—O bond scission (Fig. 3I). The magnetic moment and electronic state of single metal atoms in SACs could also be modulated through the incorporation of a second atom, which may change the adsorption energy of intermediates and improve the ORR performance. For instance, DFT calculations performed by Sun *et al.* (*97*) showed decreased magnetic moment and increased valence electrons of single–Fe atom sites after B doping, thus greatly boosting the ORR activity. In the work conducted by Wang and co-workers (*98*), the incorporation of atomically dispersed Fe and Co dual-atom active sites into two-dimensional (2D) conjugated aromatic networks [CAN-Pc(Fe/Co)] resulted in an increased content of low-spin Fe^{2+} in Fe-N_4 moiety (Fig. 3J), which largely facilitated the ORR process.

All these results from recent advances demonstrate the rational manipulation of microenvironment of single-atom sites as an essential way for developing highly efficient single-atom ORR catalysts. Moreover, it is of great importance to identify the intrinsic reactive centers in SACs under practical catalysis condition for rational design of high-performance SACs.

Oxygen evolution reaction

The OER, which involves multiproton-coupled electron transfer steps, is an essential half-reaction for rechargeable metal-air battery and water splitting. The application of SACs such as SAAs and layered double hydroxide (LDH)/carbon–supported SACs in OER electrocatalysis has been widely reported. Engineering the microenvironment of SACs has been proven as an effective method to boost the sluggish kinetics of OER.

SAAs, with adjustable electronic structure of single-atom sites, have attracted great interest as OER catalysts. In the work conducted by Li *et al.* (*99*), a series of $PtCu_x/Pt_{skin}$ core-shell structures with atomically dispersed Ru_1 (Ru_1-Pt_xCu_{4-x} SACs) were synthesized and the origin of their enhanced OER performance was unraveled. A volcano relation between the lattice constant and OER activity was demonstrated. The calculated volcano plot of OER overpotential η with $\Delta G_O - \Delta G_{OH}$ and ΔG_{OH} on the Ru_1-Pt_xCu_{4-x} (111) SACs is shown in Fig. 4A. A weak binding of adsorbate over the single–Ru atom site increases the dehydrogenation barrier, while a strong binding is detrimental for the formation of *OOH intermediate and the subsequent O_2 generation. The projected density of states of Ru_1 was found to be shifted gradually toward the Fermi level with increasing Pt-to-Cu ratio in Pt_xCu_{4-x} owing to the gradual release of compressive surface strain with respect to the pristine Pt (Fig. 4B). As a result, the tailored electronic structure of single Ru sites, which is engineered via the compressive strain of Pt_{skin} shell, has been proven critical for the optimized binding of oxygenated species and the improved OER activity and stability.

The OER performance could also be tailored through anchoring different metal atoms. For instance, by DFT calculations, Xu *et al.* screened 28 single metal atoms supported on MoS_2 edges as OER catalysts (*100*). The Pt/T1 vacancy termination in Pt_1-doped MoS_2 was found to have minimum theoretical overpotential for OER (Fig. 4, C and D). In addition, the S coordination environment and electronegativity of the single-atom sites are confirmed as a structure descriptor for the adsorption-activity-structure relationship of MoS_2-based SACs. In the work done by Li *et al.* (*101*), single Ru atoms dispersed on the surface of CoFe LDHs (Ru_1/CoFe-LDHs SAC) were developed for electrocatalytic OER, and the formation of *OOH group was determined as the rate-determining step (Fig. 4E). Further in situ/operando results indicate the strong synergetic electron coupling between LDH substance and single Ru atoms, which avoided the formation of the high oxidation state of Ru and optimized the adsorption free energy of *OOH, boosting the OER activity. Recently, Yan *et al.* (*102*) developed a single W atom–doped $Ni(OH)_2$ nanosheet [W_1-doped $Ni(OH)_2$] SAC for OER. DFT calculations show that both O—O coupling and O radical can be generated at the single–W atom site (Fig. 4F), owing to the low spin population of d^0 W^{6+}. In addition, DFT calculations carried out by Lai *et al.* (*103*) suggest that Ir_1@CoO (Ir) in Ir_1@Co/NC SAC is responsible for the high OER performance (Fig. 4G). In the work performed by Cai *et al.* (*104*), the annealed Au@Ni_2P sample with formation of tiny Au clusters and single Au atoms on Ni_2P exhibited outstanding OER activity (Fig. 4H).

Carbon matrix is a common support used for preparing SACs with controlled microenvironment for OER. For instance, atomically distributed Ni sites anchored on N-doped hollow carbon matrix with unsaturated coordination geometry show high OER performance with excellent stability (*105*). The electronic coupling via the Ni-N coordination can move down the Fermi level of single–Ni atom sites, which effectively lowers the adsorption energy of reaction intermediates and, thus, boosts OER kinetics (Fig. 4I). In the work conducted by Cao *et al.* (*106*), the O-Ru_1-N_4 structure formed through pre-adsorption of O atom on Ru-N-C SAC was demonstrated with a low O—O coupling barrier for the formation of *OOH intermediate, which is responsible for the high OER performance (Fig. 4, J and K). In addition, as the synergistic effect of neighboring dual-metal sites helps to optimize the adsorption/desorption of reactive intermediates (Fig. 4, L and M) (*107*), development of atomically dispersed binary sites on carbon hosts offers another promising way to decrease the overall reaction barrier for OER.

Hydrogen evolution reaction

Electrochemical water splitting through HER provides a sustainable and green route to produce molecular hydrogen (H_2) for mitigating the global energy crisis; however, the development of active catalysts with minimal overpotential and high efficiency is still urgently demanded for its large-scale application. Recently, SACs supported on various kinds of materials including MoS_2, MXene, and carbon-based matrix have been widely used to catalyze HER (*108*–*110*). Microenvironment engineering of atomically dispersed active sites, which can result in unique structures and electronic properties of SACs, has been proven as a promising way to dramatically accelerate the reaction kinetics of HER.

The HER activity could be improved by designing large numbers of well-defined atomically dispersed active sites hosted over transition metal dichalcogenide materials, such as MoS_2 (*111*–*115*). For instance, carbonized polyacrylonitrile-immobilized single molecular MoS_2 (MoS_2-cPAN) was demonstrated with much higher turnsover frequency (TOF) to HER than bulk MoS_2 (Fig. 5A) (*116*). Qi *et al.*

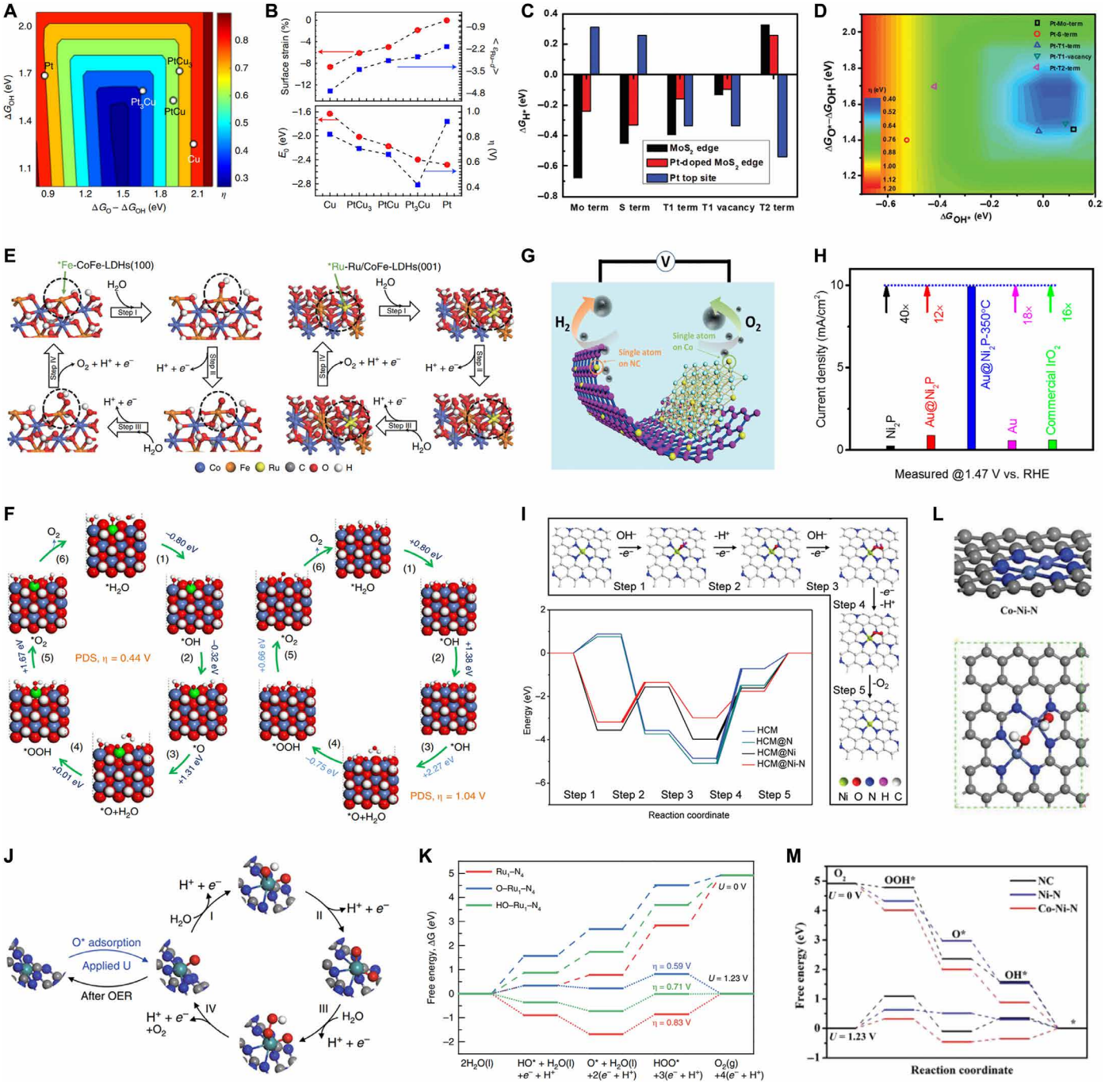

Fig. 4. Applications of SACs in OER. (**A**) Calculated volcano plot of OER overpotential η with $\Delta G_O - \Delta G_{OH}$ and ΔG_{OH} on Ru_1-Pt_xCu_{4-x} (111) SACs, (**B**) in-plane lattice contraction relative to the Pt(111) pristine surface (red circles) and d-band center of Ru_1 (blue squares), together with the corresponding adsorption η (blue squares) and energy E_0 of the oxygen atoms (red circles), adapted with permission from Yao *et al*. (*99*). (**C**) The hydrogen Gibbs free energy on Pt-doped edge (red bar), Pt top site (blue bar), and pure MoS_2 edge (black bar); (**D**) theoretical overpotentials for the Pt-doped MoS_2 terminations as a function of ΔG_{OH}* and ΔG_O* − ΔG_{OH}*, adapted with permission from Xu *et al*. (*100*). (**E**) Proposed 4e^- OER mechanism on CoFe-LDHs and Ru_1/CoFe-LDHs SAC, adapted with permission from Li *et al*. (*101*). (**F**) Proposed OER mechanism on W_1-doped $Ni(OH)_2$ SAC and bare $Ni(OH)_2$ catalyst, adapted with permission from Yan *et al*. (*102*). (**G**) Proposed OER mechanism on M_1@Co/NC SACs (M = Ir, Fe, Ni, Pt, Ru, and Pd), adapted with permission from Lai *et al*. (*103*). (**H**) OER current density at 1.47 V versus RHE of Ni_2P matrix–supported single Au atoms and tiny clusters, adapted with permission from Cai *et al*. (*104*). (**I**) Proposed OER mechanism over HCM@Ni-N SAC and free energy diagram at 0 V versus RHE, adapted with permission from Zhang *et al*. (*105*). (**J**) Proposed OER mechanism over Ru-N-C SAC in acidic electrolyte, (**K**) free energy diagram for OER on O-Ru_1-N_4 (blue line), HO-Ru_1-N_4 (green line), and Ru_1-N_4 (red line), adapted with permission from Cao *et al*. (*106*). (**L**) Co-Ni-N models. (**M**) Free energy diagram for OER on NC, Ni-N, and Co-Ni-N, adapted with permission from Han *et al*. (*107*).

(*117*) recently developed an interface SAC with atomic cobalt array bound to distorted 1T MoS_2 (Co-MoS_2) that achieves Pt-like HER activity with high catalytic stability. DFT calculation results show the ensemble effect via the synergy of S and Co in the distorted 1T MoS_2 support (Fig. 5, B and C), which changes the hydrogen-binding mode. In addition, substitution of Mo by Ni in MoS_2 with formation of positively charged Ni-S centers greatly modified the electronic structure of Ni-MoS_2 SAC and, thus, improved the hydrogen evolution activity (*113*).

MXenes have been recently applied as promising hosts for anchoring single metal atoms with controlled microenvironment for boosting HER (*118*, *119*). In the work done by Zhang *et al.* (*47*), electrochemical, exfoliated, double transition metal MXene nanosheets ($Mo_2TiC_2T_x$) were used to immobilize single Pt atoms for enhancing HER performance. The replacement of a Mo atom by a single Pt atom, which causes a reduced charge density around Pt atom due to charge delocalization from Pt to the surrounding atoms (Fig. 5D), greatly reduces the adsorption energy for H^+ (Fig. 5E) and, thus, facilitates the formation and release of molecular hydrogen. Recently, a titanium carbide ($Ti_3C_2T_x$) MXene was used by Ramalingam *et al.* (*120*) to host single Ru atoms coordinated with N and S sites (Ru_{SA}-N-S-$Ti_3C_2T_x$ SAC), which displayed superior HER activity. DFT calculations suggest that the N and S co-coordinated single Ru sites have optimal Gibbs hydrogen adsorption free energy (ΔG_H*) (Fig. 5F). Furthermore, as demonstrated by Kuznetsov *et al.* (*119*), anchoring of isolated Co atoms on Mo vacancies in the oxygen-terminated 2D molybdenum carbide (Mo_2CT_x) could also tailor the binding of hydrogen and, thus, enhance the HER kinetics.

Recently, many strategies such as construction of nonmetal SACs (*121*) and SAA catalysts (*122*) and development of hosts for anchoring single metal atoms (*123*) have been reported for improving the HER performance. In a recent work done by Jiang *et al.* (*124*), single Pt atom embedded in nanoporous cobalt selenide (Pt/np-$Co_{0.85}Se$ SAC) was developed as an efficient electrocatalyst for HER. Fourier transform EXAFS result indicates that the Pt atoms, which occupy the Co vacancies and coordinate with Se atoms, have a positive valence state due to the electron transfer from Pt to Se. DFT calculations show that the electronic interactions between np-$Co_{0.85}Se$ and atomic-level Pt can largely improve adsorption/desorption of hydrogen, thus reduce the energy barriers for water dissociation, and promote the HER kinetics (Fig. 5G).

Microenvironment engineering of atomically dispersed metal sites anchored on various carbon-based hosts has also attracted great interest in HER (*125*–*133*). For instance, Liu *et al.* (*134*) developed onion-like nanospheres of carbon (OLC)–supported single Pt atom (Pt_1/OLC SAC) as a highly efficient HER catalyst. A remarkable enrichment of protons around single Pt atoms was identified (Fig. 5H). The tip-enhancement effect at the single–Pt atom site, inducing strong localized electric field and extracting electrons from the support, was considered as the main factor for enhancing the HER activity. In the work done by Xue *et al.* (*135*), zero valent single Ni/Fe atoms anchored on graphdiyne were developed for hydrogen evolution. The real-space highest occupied molecular orbital (HOMO) and lowest unoccupied molecular orbital (LUMO) contour plots on Ni-on-GD SAC as shown in Fig. 5I clearly demonstrate the charge density distributions induced by a single Ni^0 atom. The strong electronic coupling and chemical interactions between different electronically active C sites of Graphdiyne (GD) and the single Ni/Fe atoms (Fig. 5J) largely improved the HER performance.

Recently, Cao *et al.* (*136*) developed a phosphorized carbon nitride–immobilized single–Co atom catalyst (Co_1/PCN SAC) with uniform Co_1-N_4 moiety for HER. Operando XAFS measurements reveal that the formation of high-valence HO-Co_1-N_2 moiety, followed by the preferred dynamic H_2O adsorption as H_2O-(HO-Co_1-N_2), accelerates the H_{ad} adsorption.

Co_2 reduction reaction

The electrochemical CO_2RR offers a viable strategy to decrease CO_2 emissions and mitigate the energy crisis (*4*, *12*, *137*, *138*). SACs have shown excellent activity and selectivity in CO_2RR for the conversion of CO_2 into value-added chemicals such as CO, formic acid, C_2 products, etc. (*31*, *139*–*143*). Microenvironment engineering of SACs offers great opportunities for reducing the overpotential of CO_2RR and improving the selectivity for the desired products. Moreover, the SACs with well-controlled coordination environment and electronic state provide a platform to understand the structure-activity relationship of the reactive sites and the underlying reaction mechanism, which is of great importance for practical application of electrocatalytic CO_2RR.

Fe-based SACs with various microenvironments have been demonstrated to be promising for CO_2RR (*144*–*147*). For instance, by investigating a series of iron-based catalysts for the electroreduction of CO_2 to CO, Huan *et al.* (*146*) identified the isolated FeN_4 sites as the critical catalytic species. In the work performed by Qin *et al.*, by combining DFT calculations and in situ infrared absorption spectroscopy investigations, the edge-hosted Fe_{2+2} sites embedded in a defective graphitic layer have been shown as the real active sites for CO_2-to-CO electrocatalytic conversion (*144*). The electronic state of the single-atom sites is also a main factor determining the electrocatalytic performance of CO_2RR. As shown in Fig. 6A, for the Fe-based SACs with Fe^{3+} ions, negligible shift of the Fe K-edge could be observed at −0.4 V (versus Reversible Hydrogen Electrode, RHE), indicating that the oxidation state of Fe^{3+} ions remained unchanged during CO_2RR. However, the Fe K-edge shifted to lower energies at −0.5 V (versus RHE) and beyond, the same potential for the deactivation of Fe^{3+}-N-C, implying that Fe^{3+} sites in Fe-based SACs are more active for CO_2RR (*147*).

Ni-based SACs with various coordination environments and electronic states have also been demonstrated to be efficient for CO_2RR (*148*–*155*). The adsorption energies of *CO and *COOH on single-atom sites could be largely affected by the microenvironment of single-atom sites, thus determining the CO_2RR performance. For instance, DFT calculations carried out by Zhao *et al.* (*156*) suggest that the formed *COOH can be easily reduced to CO* for both NiN_x (x = 1 to 4) and the Ni_{309} cluster (Fig. 6B); however, the *CO desorption from the Ni_{309} cluster is much more difficult than that from NiN_x, indicating NiN_x as the real active species for CO_2RR. In the work conducted by Liu and colleagues, atomically dispersed Ni(I) has been proven as the active site for CO_2RR (*55*); the as-developed single–Ni atom catalyst exhibits high intrinsic activity for CO_2 reduction, reaching a TOF of 14,800 $hours^{-1}$ with 97% Faradaic efficiency at a mild overpotential of 0.61 V. The following research from the same group further identified the high activity of Ni^+ in a model Ni-based SAC for CO_2 activation through operando XAS and Raman measurements (Fig. 6C) (*66*).

Co-based SACs have also been recognized as promising catalysts for CO_2RR (*4*, *157*–*159*). As shown in Fig. 6 (D and E), DFT calculations on well-defined metal N_4 sites reveal that CoN_4 species

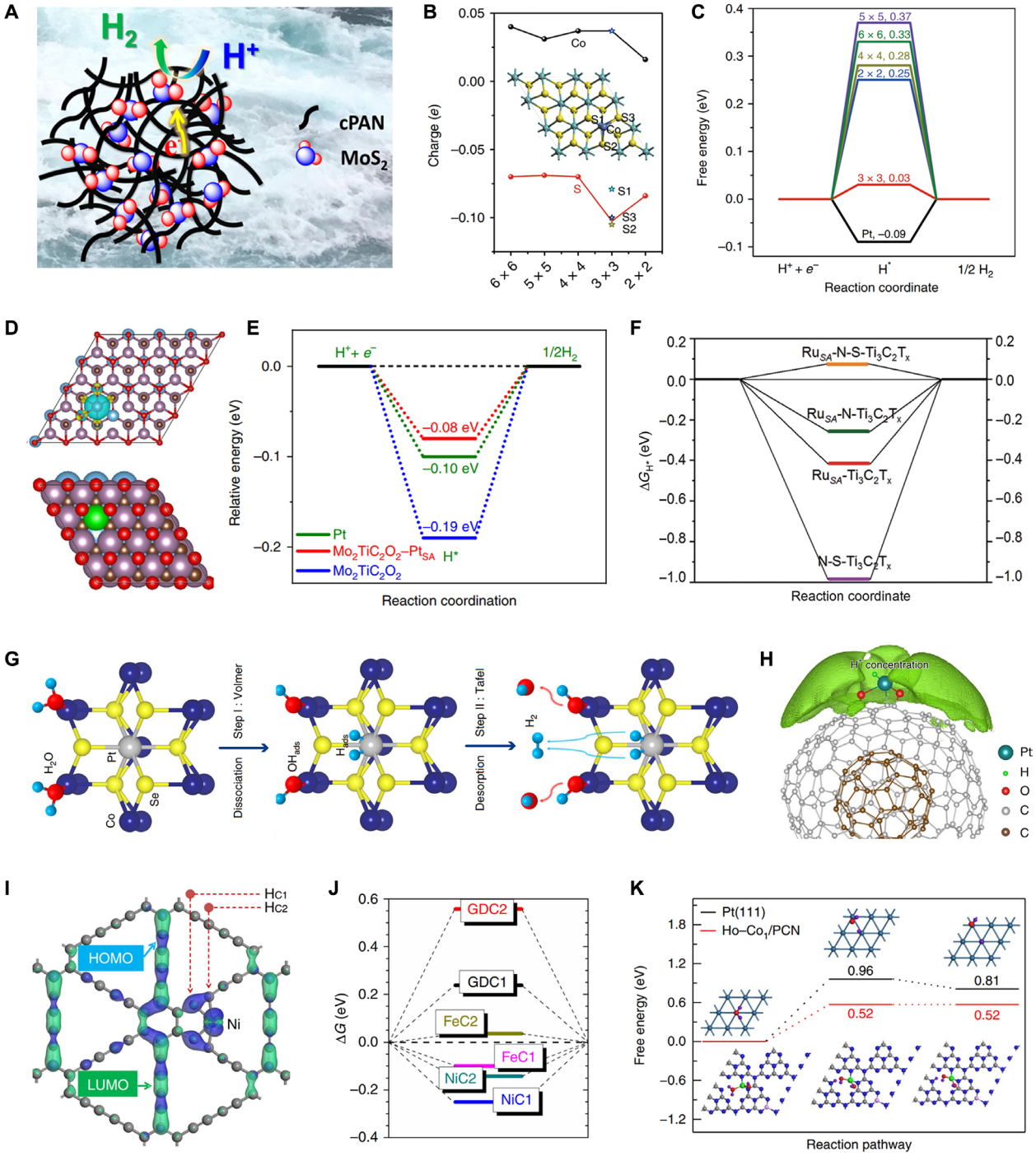

Fig. 5. Applications of SACs in HER. (**A**) Immobilized single molecular MoS_2 on carbonized polyacrylonitrile for HER, adapted with permission from Zeleke *et al.* (*116*). (**B**) The electron charge of a single Co atom and adjacent S as a function of Co coverage in Co-MoS_2 SAC, (**C**) calculated free energy diagram of HER for Co-MoS_2 SAC with different atomic Co loading amounts, adapted with permission from Qi *et al.* (*117*). (**D**) DFT models used to describe Pt-$Mo_2TiC_2O_2$ SAC, (**E**) calculated free energy diagram for HER on Pt/C, Pt-$Mo_2TiC_2O_2$ SAC, and $Mo_2TiC_2O_2$, adapted with permission from Zhang *et al.* (*47*). (**F**) Calculated free energy diagram of HER for N-S-$Ti_3C_2T_x$, Ru_{SA}-N-$Ti_3C_2T_x$, Ru_{SA}-$Ti_3C_2T_x$, and Ru_{SA}-N-S-$Ti_3C_2T_x$ catalysts, adapted with permission from Ramalingam *et al.* (*120*). (**G**) Schematic illustration of the HER mechanism over single platinum atoms embedded in nanoporous cobalt selenide (Pt/np-$Co_{0.85}Se$ SAC) in neutral media, adapted with permission from Jiang *et al.* (*124*). (**H**) HER catalyzed by atomically dispersed Pt, supported on onion-like nanospheres of carbon (Pt_1/OLC SAC), adapted with permission from Liu *et al.* (*134*). (**I**) Real-space highest occupied molecular orbital (HOMO) and lowest unoccupied molecular orbital (LUMO) contour plots on Ni-on-GD SAC, and the H_{C1} and H_{C2} denote the active H adsorption sites labeled with C_1 and C_2, respectively. (**J**) The free energy profile (ΔG) with respect to the chemisorption energy of H for HER, adapted with permission from Xue *et al.* (*135*). (**K**) Calculated energy diagram for H_2O dissociation on HO-Co_1/PCN SAC and Pt(111), adapted with permission from Cao *et al.* (*136*).

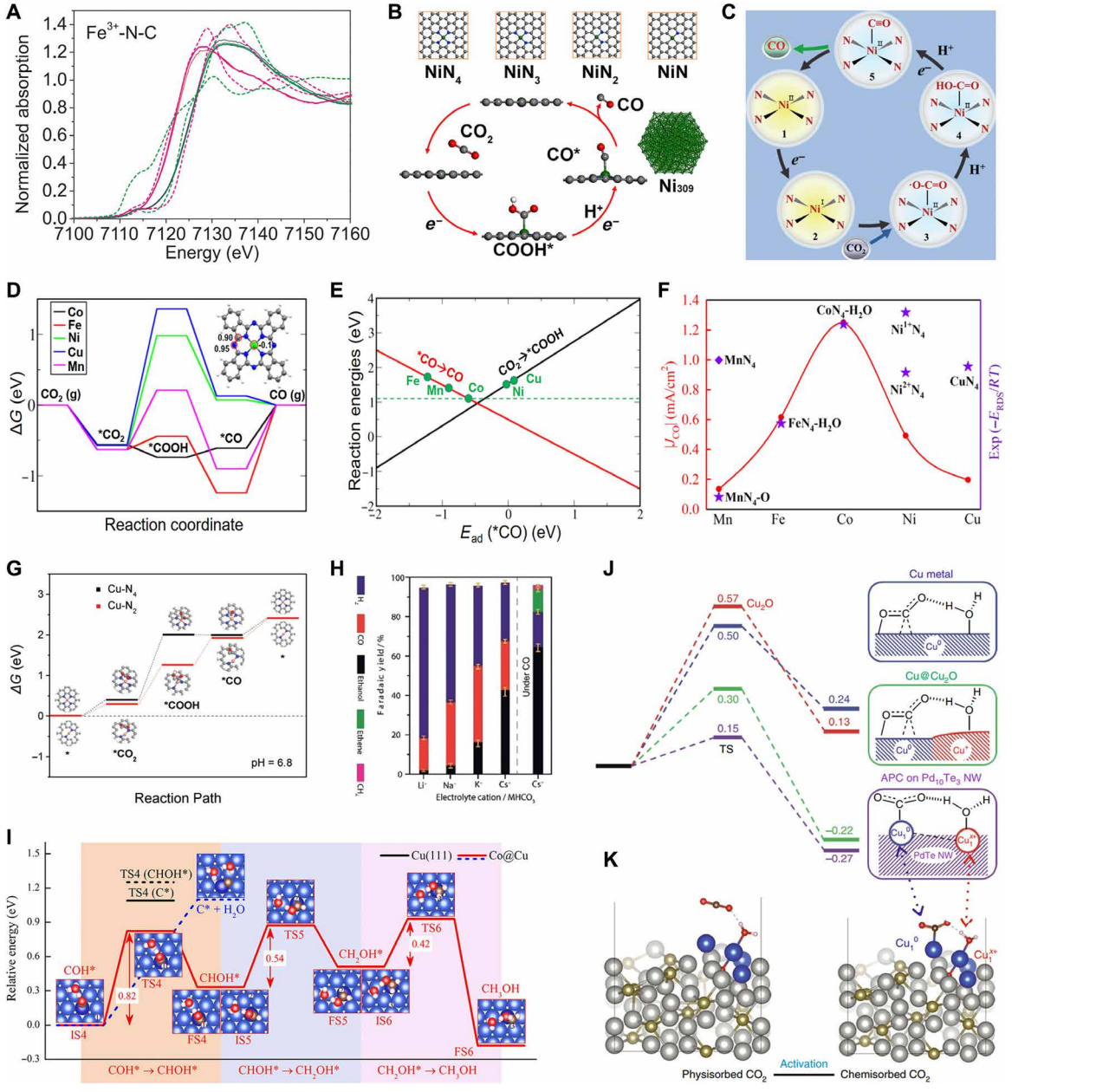

Fig. 6. Applications of SACs in CO_2RR. (**A**) Operando XAS characterization of CO_2RR over Fe^{3+}-N-C SAC, adapted with permission from Gu *et al.* (*147*). (**B**) Proposed CO_2RR pathways on optimized atomic structures of different NiN_x structures and the Ni_{309} cluster, adapted with permission from Zhao *et al.* (*156*). (**C**) Proposed CO_2RR pathway on the Ni-N-C SAC, adapted with permission from Liu *et al.* (*66*). (**D**) Calculated free energy diagram of CO_2RR for the MePc electrode, (**E**) fitted *CO desorption, and *COOH formation trends over the MePc electrode, adapted with permission from Zhang *et al.* (*61*). (**F**) Comparison of DFT calculated trends for pyrolyzed metal–nitrogen–carbon (MNC) materials and experimental CO partial current density recorded at −0.6 V (versus RHE), adapted with permission from Li *et al.* (*160*). (**G**) Free energy profiles for CO_2RR over Cu-N_2 and Cu-N_4 models, adapted with permission from Zheng *et al.* (*164*). (**H**) Faradaic yields of CO_2RR over $Cu_{0.5}$-NC SAC at −1.2 V versus RHE, adapted with permission from Karapinar *et al.* (*165*). (**I**) Relative energy diagram for the reduction of COH* to CH_3OH under zero voltage over Co@Cu SAA, adapted with permission from Zhao and Lu (*166*). (**J**) Free energy profiles for CO_2RR at −0.78 V versus RHE over Cu metal, Cu@Cu_2O, and Cu-APC on $Pd_{10}Te_3$ nanowires, (**K**) Configurations of physisorbed and chemisorbed CO_2 on Cu-APC, adapted with permission from Jiao *et al.* (*40*).

exhibit the optimum activity for CO_2 reduction to CO due to the moderate binding energy for both *CO and *COOH on the single–Co atom sites (*61*). In addition, a volcano trend between the nature of metal N_4 sites and their activities toward CO formation, with Fe and/or Co at the top of the volcano, was identified by Li and co-workers (Fig. 6F) (*160*). Detailed electronic structure analysis suggests that the enhanced catalytic activity of Co-based SACs with coordinating N atoms substituted by O or C atoms is due to the lack of π bonding in the Co—O bond compared to the Co—N or Co—C bond (*158*).

Other transition metal–based SACs such as Cu, Zn, Mn, etc. have also been studied for CO_2RR (*161*–*163*). Zheng *et al.* (*164*)

demonstrated the atomically dispersed Cu-N_2 active sites in ultrathin Cu-N_2/GN nanosheets as the real active species for CO_2RR. As shown in Fig. 6G, the optimized reaction-free energy for CO_2 activation over Cu-N_2 sites promotes the electron transfer from the single–Cu atom sites to *CO_2, thus boosting the *COOH generation. In the work done by Karapinar *et al.* (*165*), Cu-SAC with a CuN_4 coordination environment was developed for CO_2RR, achieving a Faradaic yield of 55% for ethanol under optimized conditions (Fig. 6H). Operando XAS experiments established the very small metallic Cu nanoparticles converted from the CuN_4 sites during electrolysis as the active species for the unique reactivity. Recently, Cu-based SAA has been theoretically shown as a promising catalyst for electrochemical reduction of CO_2 to methanol at a low overpotential (*166*). As shown in Fig. 6I, the formation of the free atom-like d-band due to the isolated metal atoms could modulate the adsorption strength of reaction intermediates, thus leading to the efficient formation of CH_3OH.

The recent advances for the application of SACs in CO_2RR indicate that the C—C coupling is rather difficult on single active metal sites. Therefore, the rational design SACs with dual active sites has been considered as a promising approach to improve the catalytic performance and generate C_2 products through optimizing the adsorption energies for *CO and *COOH (*73*). For instance, an APC featuring a stable Cu_1^0-Cu_1^{x+} pair structure was developed for CO_2RR by Li and co-workers (*40*). Experimental characterization and DFT calculation revealed that the Cu_1^{x+} site could adsorb H_2O while the Cu_1^0 site could adsorb CO_2 (Fig. 6, J and K), which boosted the CO_2 activation. In the work conducted by Qiao and co-workers (*167*), by using C_3N_4 as a molecular scaffold to modify the electronic structure of supported Cu atoms, the adsorption behavior of reaction intermediates could be optimized, which resulted in the unique capability to generate C2 products. A dual active center mechanism, which illustrates the single Cu active center for carbon and C-containing species adsorption and the adjacent C atom on g-C_3N_4 for bonding reaction intermediates having oxygen (such as *OCH_2, *OCH_3, *O, and *OH), was theoretically evidenced.

Nitrogen reduction reaction

The electrocatalytic NRR has been considered as an attractive route for nitrogen fixation and ammonia production. However, the large overpotential and low faradic efficiency toward NH_3, as two major issues, largely limit the further development of NRR. Owing to the unique structural and electronic features, SACs have attracted increasing attention in exploring advanced NRR electrocatalysts and revealing the underlying mechanisms. By rationally designing the microenvironment of different metal centers with diverse supports, SACs are promising to improve the catalytic performance and understand the microenvironment-activity relationships for efficient NRR.

Recently, by using DFT calculations, Qiao and co-workers built up a library of different transition metal centers anchored on various NC as NRR catalysts, which illustrates the electronic origins, activity trends, and design strategies of SACs for electrocatalytic N_2 reduction (*168*). As shown in Fig. 7A, the maximum activity for NRR, marked by the red region, could be possibly achieved by independently tuning ΔG_{NNH}* and ΔG_{NH2}*. Since the supports or ligands of the active centers could regulate the scaling relations for intermediate adsorption, the rationally designed SACs with controlled microenvironment is shown to be critical for improving the catalytic activity. In addition, the stability of the ligands should also be considered to ensure the durability of NRR SACs. As shown in Fig. 7B, the decomposition potentials for g-C_3N_4, four coordinating nitrogen atoms (N_4), and three coordinating nitrogen atoms (N_3) were calculated to be −0.81, −1.03, and −0.71 V (versus Standard Hydrogen Electrode, SHE), respectively, indicating the high stability of SACs supported on the NC substrate under moderate NRR potential. Results of this work predicted Ru@g-C_3N_4 close to the ideal region as a promising candidate for NRR, which has been experimentally verified (*169*–*171*). As evidenced by Yu *et al.* (*169*), the doping of single Ru atoms could lead to notable electronic rearrangement of both g-C_3N_4 and Ru atoms (Fig. 7C), which led to stronger N_2 adsorption on Ru SAs/g-C_3N_4 compared to that on Ru bulk surface and, thus, improved the catalytic activity and selectivity for NH_3 formation. In the work conducted by Sun and colleagues (*170*), the single Ru atoms anchored in oxygen vacancies have been shown as the main active centers for NRR, which enable the stabilization of *NNH and enhance the N_2 adsorption (Fig. 7D). Both Ru@$Zr_{32}O_{63}$ and Ru/NC_2 SACs were demonstrated to be highly active for NRR because of the reduced free energy for *NNH formation (Fig. 7, E and F), which is considered as the most energy-consuming step in electrochemical NRR.

SACs with other single-atom centers (Fe, Co, Mo, B, etc.) have also been investigated in NRR (*172*–*180*). For instance, Ou *et al.* (*181*) systematically studied the Gibbs free energies for *H (ΔG^*_H) and *N_2 (ΔG^*_{N2}) on various Mo-based SACs. As shown in Fig. 7 (G and H), Mo_1N_3 anchored on N-doped black phosphorus, with extremely low overpotential (0.02 V) and fast removal of the NH_3 molecule, is proposed as a compelling highly efficient catalyst for NRR. Recently, a type of SACs with single V atoms anchored on boron monolayer (V/β_{12}-BM) was theoretically evidenced as a promising catalyst for NRR (*182*). As shown in Fig. 7 (I and J), by calculating the free energy change of each elementary step over V/β_{12}-BM SAC during NRR, an "acceptance-donation" interaction between the V atom and N_2 was proposed. The ionization of 1π orbital of N_2, which greatly elongates the N—N bond length, leads to the enhanced activity for electrocatalytic N_2 reduction. In the work conducted by Sun and co-workers (*183*), single B atoms anchored on different 2D materials were theoretically studied as electrocatalysts for NRR (Fig. 7K). The volcano diagrams for NRR over different B-based SACs as shown in Fig. 7L indicate that the catalytic activity of boron is highly correlated with the charge transfer degree between the substrate and the boron atom. Results of this work identified the single boron atoms substituted into h-MoS_2 (hS-1) and supported on graphene (G-A) as the most promising NRR catalyst. All these results provide a general guideline for the rational design of efficient SACs for electrocatalytic N_2 reduction through microenvironment engineering.

SUMMARY AND OUTLOOK

In summary, we have witnessed the fast development of SACs in both their preparation strategies and application field in electrochemical energy conversion. A number of synthetic strategies including defect engineering, spatial confinement, atomic alloying, molecular bridging, MOF derivatization, etc. have been categorized for the synthesis of SACs with various microenvironments. The distinct atomic local microenvironment of SACs offers remarkable advantages of distinguished activity, selectivity, and stability for a wide variety of electrochemical reactions such as ORR, HER, OER, NRR, and CO_2RR. Furthermore, the microenvironment modulation

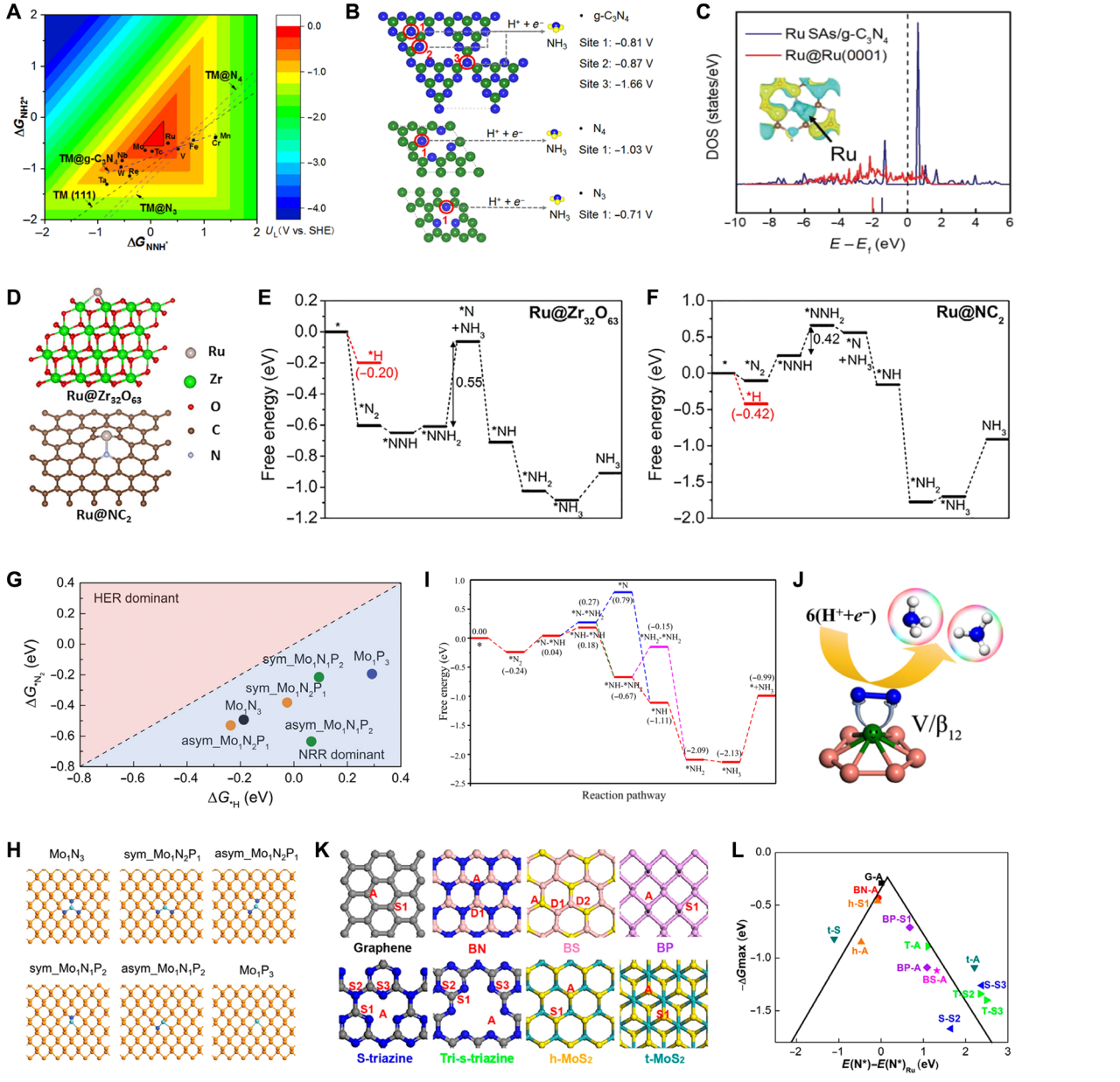

Fig. 7. Applications of SACs in NRR. (**A**) Comparison of the limiting potential as a function of Gibbs free energy of *NH_2 (ΔG_{NH2}*) and *NNH (ΔG_{NNH}*) for SACs consisting of different metal centers and supports and (**B**) decomposition energies of N-doped supports (NC and g-C_3N_4 with three or four nitrogen atoms as the coordinating sites), adapted with permission from Liu *et al*. (*168*). (**C**) Calculated projected density of states of *d* electrons of a Ru atom on Ru (0001) surface and Ru SAs/g-C_3N_4, adapted with permission from Yu *et al*. (*169*). (**D**) DFT models for Ru/NC_2 and Ru@$Zr_{32}O_{63}$, (**E**) free energy diagram for NRR over Ru@$Zr_{32}O_{63}$, and (**F**) free energy diagram for NRR over Ru/NC_2, adapted with permission from Tao *et al*. (*170*). (**G**) Gibbs free energies for *N_2 (ΔG*$_{N2}$) and *H (ΔG*$_H$) of Mo-based SACs and (**H**) optimized configurations of Mo-based SACs, adapted with permission from Ou *et al*. (*181*). (**I**) Free energy diagram for NRR over single V atom anchored on boron monolayer (V/β_{12}-BM) and (**J**) mechanism for NRR over V/β_{12}-BM, adapted with permission from Zhu *et al*. (*182*). (**K**) Proposed atomic model of single B atom anchored on different 2D materials and (**L**) volcano diagrams for NRR over single–B atom catalysts, adapted with permission from Liu *et al*. (*183*).

of SACs would provide great help in the deep understanding of the microenvironment-activity relationships and underlying catalytic mechanisms associated to different electrochemical reactions.

However, the research of microenvironment engineering of SACs for electrochemical energy conversion is still at its infancy stage. First, although many advanced strategies have been proven to be powerful for altering the microenvironments of SACs, the development of novel synthesis strategies for the "precise control" of the microenvironments in SACs is still challenging but highly desired. Second, despite the fact that many efforts have been devoted to studying the carbon-based SACs, microenvironment engineering of single atoms on many other types of hosts, such as MXenes, transition metal dichalcogenide materials, defective metal oxides, as well as single atom alloys, deserves more attention. Third, theoretical

prediction based on computational modeling has been proven useful in discovering SACs for electrochemical applications. Strategies for the rational design of model SACs with a well-controlled microenvironment based on the DFT studies are still highly desired. Last, SACs provide an ideal platform for investigating the microenvironment-activity relationships and the underlying reaction mechanisms of various electrochemical energy conversion reactions. In most cases, although the catalytic center is stable during the reaction, the microenvironment of SACs would undergo a dynamic cycle with in situ formation of intermediate species; therefore, the integrated utilization of in situ/operando techniques is of significance but still under development.

As a conclusion, despite that the exciting advances have been achieved in the microenvironment engineering of SACs for electrochemical energy conversion, opportunities and challenges are both to be faced. Therefore, microenvironment engineering of SACs with a well-controlled coordination environment and electronic state, integrated with the advanced in situ/operando techniques as well as DFT theoretical studies, shall pave the way for both fundamental research and the future industrial applications of SACs for various electrochemical energy conversion fields.

REFERENCES AND NOTES

1. M. K. Debe, Electrocatalyst approaches and challenges for automotive fuel cells. *Nature* **486**, 43–51 (2012).
2. T. R. Karl, K. E. Trenberth, Modern global climate change. *Science* **302**, 1719–1723 (2003).
3. S. Lin, C. S. Diercks, Y.-B. Zhang, N. Kornienko, E. M. Nichols, Y. Zhao, A. R. Paris, D. Kim, P. Yang, O. M. Yaghi, C. J. Chang, Covalent organic frameworks comprising cobalt porphyrins for catalytic CO_2 reduction in water. *Science* **349**, 1208–1213 (2015).
4. S. Ren, D. Joulié, D. Salvatore, K. Torbensen, M. Wang, M. Robert, C. P. Berlinguette, Molecular electrocatalysts can mediate fast, selective CO_2 reduction in a flow cell. *Science* **365**, 367–369 (2019).
5. Z. W. Seh, J. Kibsgaard, C. F. Dickens, I. Chorkendorff, J. K. Nørskov, T. F. Jaramillo, Combining theory and experiment in electrocatalysis: Insights into materials design. *Science* **355**, eaad4998 (2017).
6. B. Zhang, X. Zheng, O. Voznyy, R. Comin, M. Bajdich, M. García-Melchor, L. Han, J. Xu, M. Liu, L. Zheng, F. Pelayo García, de Arquer, C. T. Dinh, F. Fan, M. Yuan, E. Yassitepe, N. Chen, T. Regier, P. Liu, Y. Li, P. De Luna, A. Janmohamed, H. L. Xin, H. Yang, A. Vojvodic, E. H. Sargent, Homogeneously dispersed multimetal oxygen-evolving catalysts. *Science* **352**, 333–337 (2016).
7. M.-A. Légaré, G. Bélanger-Chabot, R. D. Dewhurst, E. Welz, I. Krummenacher, B. Engels, H. Braunschweig, Nitrogen fixation and reduction at boron. *Science* **359**, 896–900 (2018).
8. J. Li, R. Güttinger, R. Moré, F. Song, W. Wan, G. R. Patzke, Frontiers of water oxidation: The quest for true catalysts. *Chem. Soc. Rev.* **46**, 6124–6147 (2017).
9. M. Li, Z. Zhao, T. Cheng, A. Fortunelli, C.-Y. Chen, R. Yu, Q. Zhang, L. Gu, B. V. Merinov, Z. Lin, E. Zhu, T. Yu, Q. Jia, J. Guo, L. Zhang, W. A. Goddard III, Y. Huang, X. Duan, Ultrafine jagged platinum nanowires enable ultrahigh mass activity for the oxygen reduction reaction. *Science* **354**, 1414–1419 (2016).
10. D. H. Guo, R. Shibuya, C. Akiba, S. Saji, T. Kondo, J. Nakamura, Active sites of nitrogen-doped carbon materials for oxygen reduction reaction clarified using model catalysts. *Science* **351**, 361–365 (2016).
11. R. Bashyam, P. Zelenay, A class of non-precious metal composite catalysts for fuel cells. *Nature* **443**, 63–66 (2006).
12. L. Wang, W. Chen, D. Zhang, Y. Du, R. Amal, S. Qiao, J. Wu, Z. Yin, Surface strategies for catalytic CO_2 reduction: From two-dimensional materials to nanoclusters to single atoms. *Chem. Soc. Rev.* **48**, 5310–5349 (2019).
13. A. Wang, J. Li, T. Zhang, Heterogeneous single-atom catalysis. *Nat. Rev. Chem.* **2**, 65–81 (2018).
14. X. Cui, W. Li, P. Ryabchuk, K. Junge, M. Beller, Bridging homogeneous and heterogeneous catalysis by heterogeneous single-metal-site catalysts. *Nat. Catal.* **1**, 385–397 (2018).
15. X. Li, X. Yang, Y. Huang, T. Zhang, B. Liu, Supported noble-metal single atoms for heterogeneous catalysis. *Adv. Mater.* **31**, e1902031 (2019).
16. B. Qiao, A. Wang, X. Yang, L. F. Allard, Z. Jiang, Y. Cui, J. Liu, J. Li, T. Zhang, Single-atom catalysis of CO oxidation using Pt_1/FeO_x. *Nat. Chem.* **3**, 634–641 (2011).
17. L. Huang, J. Chen, L. Gan, J. Wang, S. Dong, Single-atom nanozymes. *Sci. Adv.* **5**, eaav5490 (2019).
18. S. Ding, M. J. Hülsey, J. Pérez-Ramírez, N. Yan, Transforming energy with single-atom catalysts. *Joule* **3**, 2897–2929 (2019).
19. R. Lin, D. Albani, E. Fako, S. K. Kaiser, O. V. Safonova, N. López, J. Pérez-Ramírez, Design of single gold atoms on nitrogen-doped carbon for molecular recognition in alkyne semi-hydrogenation. *Angew. Chem. Int. Ed.* **58**, 504–509 (2019).
20. E. Vorobyeva, E. Fako, Z. Chen, S. M. Collins, D. Johnstone, P. A. Midgley, R. Hauert, O. V. Safonova, G. Vilé, N. López, S. Mitchell, J. Pérez-Ramírez, Atom-by-atom resolution of structure–function relations over low-nuclearity metal catalysts. *Angew. Chem. Int. Ed.* **58**, 8724–8729 (2019).
21. S. K. Kaiser, R. Lin, S. Mitchell, E. Fako, F. Krumeich, R. Hauert, O. V. Safonova, V. A. Kondratenko, E. V. Kondratenko, S. M. Collins, P. A. Midgley, N. López, J. Pérez-Ramírez, Controlling the speciation and reactivity of carbon-supported gold nanostructures for catalysed acetylene hydrochlorination. *Chem. Sci.* **10**, 359–369 (2019).
22. S. K. Kaiser, E. Fako, G. Manzocchi, F. Krumeich, R. Hauert, A. H. Clark, O. V. Safonova, N. López, J. Pérez-Ramírez, Nanostructuring unlocks high performance of platinum single-atom catalysts for stable vinyl chloride production. *Nat. Catal.* **3**, 376–385 (2020).
23. H. Fei, J. Dong, D. Chen, T. Hu, X. Duan, I. Shakir, Y. Huang, X. Duan, Single atom electrocatalysts supported on graphene or graphene-like carbons. *Chem. Soc. Rev.* **48**, 5207–5241 (2019).
24. Y. Wang, J. Mao, X. Meng, L. Yu, D. Deng, X. Bao, Catalysis with two-dimensional materials confining single atoms: Concept, design, and applications. *Chem. Rev.* **119**, 1806–1854 (2019).
25. M. T. Greiner, T. E. Jones, S. Beeg, L. Zwiener, M. Scherzer, F. Girgsdies, S. Piccinin, M. Armbrüster, A. Knop-Gericke, R. Schlögl, Free-atom-like *d* states in single-atom alloy catalysts. *Nat. Chem.* **10**, 1008–1015 (2018).
26. P. N. Duchesne, Z. Y. Li, C. P. Deming, V. Fung, X. Zhao, J. Yuan, T. Regier, A. Aldalbahi, Z. Almarhoon, S. Chen, D.-e. Jiang, N. Zheng, P. Zhang, Golden single-atomic-site platinum electrocatalysts. *Nat. Mater.* **17**, 1033–1039 (2018).
27. C. Zhu, S. Fu, Q. Shi, D. Du, Y. Lin, Single-atom electrocatalysts. *Angew. Chem. Int. Ed.* **56**, 13944–13960 (2017).
28. H. Zhang, G. Liu, L. Shi, J. Ye, Single-atom catalysts: Emerging multifunctional materials in heterogeneous catalysis. *Adv. Energy Mater.* **8**, 1701343 (2018).
29. L. Jiao, H.-L. Jiang, Metal-organic-framework-based single-atom catalysts for energy applications. *Chem* **5**, 786–804 (2019).
30. K. Jiang, H. Wang, Electrocatalysis over graphene-defect-coordinated transition-metal single-atom catalysts. *Chem* **4**, 194–195 (2018).
31. S. Mitchell, E. Vorobyeva, J. Pérez-Ramírez, The multifaceted reactivity of single-atom heterogeneous catalysts. *Angew. Chem. Int. Ed.* **57**, 15316–15329 (2018).
32. A. Beniya, S. Higashi, Towards dense single-atom catalysts for future automotive applications. *Nat. Catal.* **2**, 590–602 (2019).
33. L. Wang, M.-X. Chen, Q.-Q. Yan, S.-L. Xu, S.-Q. Chu, P. Chen, Y. Lin, H.-W. Liang, A sulfur-tethering synthesis strategy toward high-loading atomically dispersed noble metal catalysts. *Sci. Adv.* **5**, eaax6322 (2019).
34. H. Xu, D. Cheng, D. Cao, X. C. Zeng, A universal principle for a rational design of single-atom electrocatalysts. *Nat. Catal.* **1**, 339–348 (2018).
35. M. Li, K. Duanmu, C. Wan, T. Cheng, L. Zhang, S. Dai, W. Chen, Z. Zhao, P. Li, H. Fei, Y. Zhu, R. Yu, J. Luo, K. Zang, Z. Lin, M. Ding, J. Huang, H. Sun, J. Guo, X. Pan, W. A. Goddard III, P. Sautet, Y. Huang, X. Duan, Single-atom tailoring of platinum nanocatalysts for high-performance multifunctional electrocatalysis. *Nat. Catal.* **2**, 495–503 (2019).
36. W.-H. Lai, Z. Miao, Y.-X. Wang, J.-Z. Wang, S.-L. Chou, Atomic-local environments of single-atom catalysts: Synthesis, electronic structure, and activity. *Adv. Energy Mater.* **9**, 1900722 (2019).
37. Y. Zhu, J. Sokolowski, X. Song, Y. He, Y. Mei, G. Wu, Engineering local coordination environments of atomically dispersed and heteroatom-coordinated single metal site electrocatalysts for clean energy-conversion. *Adv. Energy Mater.* **10**, 1902844 (2019).
38. A. Bruix, Y. Lykhach, I. Matolínová, A. Neitzel, T. Skála, N. Tsud, M. Vorokhta, V. Stetsovych, K. Ševčíková, J. Mysliveček, R. Fiala, M. Václavů, K. C. Prince, S. Bruyère, V. Potin, F. Illas, V. Matolín, J. Libuda, K. M. Neyman, Maximum noble-metal efficiency in catalytic materials: Atomically dispersed surface platinum. *Angew. Chem. Int. Ed.* **53**, 10525–10530 (2014).
39. J. Wan, W. Chen, C. Jia, L. Zheng, J. Dong, X. Zheng, Y. Wang, W. Yan, C. Chen, Q. Peng, D. Wang, Y. Li, Defect effects on TiO_2 nanosheets: Stabilizing single atomic site Au and promoting catalytic properties. *Adv. Mater.* **30**, 1705369 (2018).
40. J. Jiao, R. Lin, S. Liu, W.-C. Cheong, C. Zhang, Z. Chen, Y. Pan, J. Tang, K. Wu, S.-F. Hung, H. M. Chen, L. Zheng, Q. Lu, X. Yang, B. Xu, H. Xiao, J. Li, D. Wang, Q. Peng, C. Chen, Y. Li, Copper atom-pair catalyst anchored on alloy nanowires for selective and efficient electrochemical reduction of CO_2. *Nat. Chem.* **11**, 222–228 (2019).
41. H. Li, S. Wang, H. Sawada, G. G. D. Han, T. Samuels, C. S. Allen, A. I. Kirkland, J. C. Grossman, J. H. Warner, Atomic structure and dynamics of single platinum atom interactions with monolayer MoS_2. *ACS Nano* **11**, 3392–3403 (2017).

42. G. Liu, A. W. Robertson, M. M.-J. Li, W. C. H. Kuo, M. T. Darby, M. H. Muhieddine, Y.-C. Lin, K. Suenaga, M. Stamatakis, J. H. Warner, S. C. E. Tsang, MoS_2 monolayer catalyst doped with isolated Co atoms for the hydrodeoxygenation reaction. *Nat. Chem.* **9**, 810–816 (2017).
43. L. Zhang, Y. Jia, G. Gao, X. Yan, N. Chen, J. Chen, M. T. Soo, B. Wood, D. Yang, A. Du, X. Yao, Graphene defects trap atomic Ni species for hydrogen and oxygen evolution reactions. *Chem* **4**, 285–297 (2018).
44. R. Lang, W. Xi, J.-C. Liu, Y.-T. Cui, T. Li, A. F. Lee, F. Chen, Y. Chen, L. Li, L. Li, J. Lin, S. Miao, X. Liu, A.-Q. Wang, X. Wang, J. Luo, B. Qiao, J. Li, T. Zhang, Non defect-stabilized thermally stable single-atom catalyst. *Nat. Commun.* **10**, 234 (2019).
45. Y. Qu, L. Wang, Z. Li, P. Li, Q. Zhang, Y. Lin, F. Zhou, H. Wang, Z. Yang, Y. Hu, M. Zhu, X. Zhao, X. Han, C. Wang, Q. Xu, L. Gu, J. Luo, L. Zheng, Y. Wu, Ambient synthesis of single-atom catalysts from bulk metal via trapping of atoms by surface dangling bonds. *Adv. Mater.* **31**, 1904496 (2019).
46. L. DeRita, J. Resasco, S. Dai, A. Boubnov, H. V. Thang, A. S. Hoffman, I. Ro, G. W. Graham, S. R. Bare, G. Pacchioni, X. Pan, P. Christopher, Structural evolution of atomically dispersed Pt catalysts dictates reactivity. *Nat. Mater.* **18**, 746–751 (2019).
47. J. Q. Zhang, Y. Zhao, X. Guo, C. Chen, C.-L. Dong, R.-S. Liu, C.-P. Han, Y. Li, Y. Gogotsi, G. Wang, Single platinum atoms immobilized on an MXene as an efficient catalyst for the hydrogen evolution reaction. *Nat. Catal.* **1**, 985–992 (2018).
48. T. Kropp, Z. Lu, Z. Li, Y.-H. C. Chin, M. Mavrikakis, Anionic single-atom catalysts for CO oxidation: Support-independent activity at low temperatures. *ACS Catal.* **9**, 1595–1604 (2019).
49. T.-Y. Chang, Y. Tanaka, R. Ishikawa, K. Toyoura, K. Matsunaga, Y. Ikuhara, N. Shibata, Direct imaging of Pt single atoms adsorbed on TiO_2 (110) surfaces. *Nano Lett.* **14**, 134–138 (2014).
50. H. Fei, J. Dong, Y. Feng, C. S. Allen, C. Wan, B. Volosskiy, M. Li, Z. Zhao, Y. Wang, H. Sun, P. An, W. Chen, Z. Guo, C. Lee, D. Chen, I. Shakir, M. Liu, T. Hu, Y. Li, A. I. Kirkland, X. Duan, Y. Huang, General synthesis and definitive structural identification of MN_4C_4 single-atom catalysts with tunable electrocatalytic activities. *Nat. Catal.* **1**, 63–72 (2018).
51. Z. Yang, B. Chen, W. Chen, Y. Qu, F. Zhou, C. Zhao, Q. Xu, Q. Zhang, X. Duan, Y. Wu, Directly transforming copper (I) oxide bulk into isolated single-atom copper sites catalyst through gas-transport approach. *Nat. Commun.* **10**, 3734 (2019).
52. Y. Qu, B. Chen, Z. Li, X. Duan, L. Wang, Y. Lin, T. Yuan, F. Zhou, Y. Hu, Z. Yang, C. Zhao, J. Wang, C. Zhao, Y. Hu, G. Wu, Q. Zhang, Q. Xu, B. Liu, P. Gao, R. You, W. Huang, L. Zheng, L. Gu, Y. Wu, Y. Li, Thermal emitting strategy to synthesize atomically dispersed Pt metal sites from bulk Pt metal. *J. Am. Chem. Soc.* **141**, 4505–4509 (2019).
53. W. Liu, L. Zhang, X. Liu, X. Liu, X. Yang, S. Miao, W. Wang, A. Wang, T. Zhang, Discriminating catalytically active FeN_x species of atomically dispersed Fe–N–C catalyst for selective oxidation of the C–H bond. *J. Am. Chem. Soc.* **139**, 10790–10798 (2017).
54. D. Xia, X. Yang, L. Xie, Y. Wei, W. Jiang, M. Dou, X. Li, J. Li, L. Gan, F. Kang, Direct growth of carbon nanotubes doped with single atomic Fe–N_4 active sites and neighboring graphitic nitrogen for efficient and stable oxygen reduction electrocatalysis. *Adv. Funct. Mater.* **29**, 1906174 (2019).
55. H. B. Yang, S.-F. Hung, S. Liu, K. Yuan, S. Miao, L. Zhang, X. Huang, H.-Y. Wang, W. Cai, R. Chen, J. Gao, X. Yang, W. Chen, Y. Huang, H. M. Chen, C. M. Li, T. Zhang, B. Liu, Atomically dispersed Ni(i) as the active site for electrochemical CO_2 reduction. *Nat. Energy* **3**, 140–147 (2018).
56. J. Zhang, Y. Zhao, C. Chen, Y.-C. Huang, C.-L. Dong, C.-J. Chen, R.-S. Liu, C. Wang, K. Yan, Y. Li, G. Wang, Tuning the coordination environment in single-atom catalysts to achieve highly efficient oxygen reduction reactions. *J. Am. Chem. Soc.* **141**, 20118–20126 (2019).
57. Y. Liu, Z. Li, Q. Yu, Y. Chen, Z. Chai, G. Zhao, S. Liu, W.-C. Cheong, Y. Pan, Q. Zhang, L. Gu, L. Zheng, Y. Wang, Y. Lu, D. Wang, C. Chen, Q. Peng, Y. Liu, L. Liu, J. Chen, Y. Li, A general strategy for fabricating isolated single metal atomic site catalysts in Y zeolite. *J. Am. Chem. Soc.* **141**, 9305–9311 (2019).
58. H. Zhang, P. An, W. Zhou, B. Y. Guan, P. Zhang, J. Dong, X. W. Lou, Dynamic traction of lattice-confined platinum atoms into mesoporous carbon matrix for hydrogen evolution reaction. *Sci. Adv.* **4**, eaao6657 (2018).
59. Y. Yin, L. Shi, W. Li, X. Li, H. Wu, Z. Ao, W. Tian, S. Liu, S. Wang, H. Sun, Boosting Fenton-like reactions via single atom Fe catalysis. *Environ. Sci. Technol.* **53**, 11391–11400 (2019).
60. Z. Zhang, Y. Chen, L. Zhou, C. Chen, Z. Han, B. Zhang, Q. Wu, L. Yang, L. Du, Y. Bu, P. Wang, X. Wang, H. Yang, Z. Hu, The simplest construction of single-site catalysts by the synergism of micropore trapping and nitrogen anchoring. *Nat. Commun.* **10**, 1657 (2019).
61. Z. Zhang, J. Xiao, X.-J. Chen, S. Yu, L. Yu, R. Si, Y. Wang, S. Wang, X. Meng, Y. Wang, Z.-Q. Tian, D. Deng, Understanding the reaction mechanisms of well-defined metal-N_4 sites in electrocatalytic CO_2 reduction. *Angew. Chem. Int. Ed.* **57**, 16339–16342 (2018).
62. X. Cui, J. Xiao, Y. Wu, P. Du, R. Si, H. Yang, H. Tian, J. Li, W.-H. Zhang, D. Deng, X. Bao, A graphene composite material with single cobalt active sites: A highly efficient counter electrode for dye-sensitized solar cells. *Angew. Chem. Int. Ed.* **55**, 6708–6712 (2016).
63. Y. Pan, R. Lin, Y. Chen, S. Liu, W. Zhu, X. Cao, W. Chen, K. Wu, W.-C. Cheong, Y. Wang, L. Zheng, J. Luo, Y. Lin, Y. Liu, C. Liu, J. Li, Q. Lu, X. Chen, D. Wang, Q. Peng, C. Chen, Y. Li, Design of single-atom Co–N_5 catalytic site: A robust electrocatalyst for CO_2 reduction with nearly 100% CO selectivity and remarkable stability. *J. Am. Chem. Soc.* **140**, 4218–4221 (2018).
64. I. Hijazi, T. Bourgeteau, R. Cornut, A. Morozan, A. Filoramo, J. Leroy, V. Derycke, B. Jousselme, S. Campidelli, Carbon nanotube-templated synthesis of covalent porphyrin network for oxygen reduction reaction. *J. Am. Chem. Soc.* **136**, 6348–6354 (2014).
65. P. Peng, L. Shi, F. Huo, C. Mi, X. Wu, S. Zhang, Z. Xiang, A pyrolysis-free path toward superiorly catalytic nitrogen-coordinated single atom. *Sci. Adv.* **5**, eaaw2322 (2019).
66. S. Liu, H. B. Yang, S.-F. Hung, J. Ding, W. Cai, L. Liu, J. Gao, X. Li, X. Ren, Z. Kuang, Y. Huang, T. Zhang, B. Liu, Elucidating the electrocatalytic CO_2 reduction reaction over a model single-atom nickel catalyst. *Angew. Chem. Int. Ed.* **59**, 798–803 (2020).
67. S. Tian, Q. Fu, W. Chen, Q. Feng, Z. Chen, J. Zhang, W.-C. Cheong, R. Yu, L. Gu, J. Dong, J. Luo, C. Chen, Q. Peng, C. Draxl, D. Wang, Y. Li, Carbon nitride supported Fe_2 cluster catalysts with superior performance for alkene epoxidation. *Nat. Commun.* **9**, 2353 (2018).
68. Z. Liang, C. Qu, D. Xia, R. Zou, Q. Xu, Atomically dispersed metal sites in MOF-based materials for electrocatalytic and photocatalytic energy conversion. *Angew. Chem. Int. Ed.* **57**, 9604–9633 (2018).
69. X. Wang, W. Chen, L. Zhang, T. Yao, W. Liu, Y. Lin, H. Ju, J. Dong, L. Zheng, W. Yan, X. Zheng, Z. Li, X. Wang, J. Yang, D. He, Y. Wang, Z. Deng, Y. Wu, Y. Li, Uncoordinated amine groups of metal–organic frameworks to anchor single Ru sites as chemoselective catalysts toward the hydrogenation of quinoline. *J. Am. Chem. Soc.* **139**, 9419–9422 (2017).
70. X. Li, X. Huang, S. Xi, S. Miao, J. Ding, W. Cai, S. Liu, X. Yang, H. Yang, J. Gao, J. Wang, Y. Huang, T. Zhang, B. Liu, Single cobalt atoms anchored on porous N-doped graphene with dual reaction sites for efficient Fenton-like catalysis. *J. Am. Chem. Soc.* **140**, 12469–12475 (2018).
71. X. Wang, Z. Chen, X. Zhao, T. Yao, W. Chen, R. You, C. Zhao, G. Wu, J. Wang, W. Huang, J. Yang, X. Hong, S. Wei, Y. Wu, Y. Li, Regulation of coordination number over single Co sites: Triggering the efficient electroreduction of CO_2. *Angew. Chem. Int. Ed.* **57**, 1944–1948 (2018).
72. J. Wang, Z. Huang, W. Liu, C. Chang, H. Tang, Z. Li, W. Chen, C. Jia, T. Yao, S. Wei, Y. Wu, Y. Li, Design of N-coordinated dual-metal sites: A stable and active Pt-free catalyst for acidic oxygen reduction reaction. *J. Am. Chem. Soc.* **139**, 17281–17284 (2017).
73. W. Ren, X. Tan, W. Yang, C. Jia, S. Xu, K. Wang, S. C. Smith, C. Zhao, Isolated diatomic Ni-Fe metal–nitrogen sites for synergistic electroreduction of CO_2. *Angew. Chem. Int. Ed.* **58**, 6972–6976 (2019).
74. L. Bai, C.-S. Hsu, D. T. L. Alexander, H. M. Chen, X. Hu, A cobalt–iron double-atom catalyst for the oxygen evolution reaction. *J. Am. Chem. Soc.* **141**, 14190–14199 (2019).
75. X. Li, X. Yang, J. Zhang, Y. Huang, B. Liu, In situ/operando techniques for characterization of single-atom catalysts. *ACS Catal.* **9**, 2521–2531 (2019).
76. C. H. Choi, M. Kim, H. C. Kwon, S. J. Cho, S. Yun, H.-T. Kim, K. J. J. Mayrhofer, H. Kim, M. Choi, Tuning selectivity of electrochemical reactions by atomically dispersed platinum catalyst. *Nat. Commun.* **7**, 10922 (2016).
77. J. Liu, M. Jiao, L. Lu, H. M. Barkholtz, Y. Li, Y. Wang, L. Jiang, Z. Wu, D.-j. Liu, L. Zhuang, C. Ma, J. Zeng, B. Zhang, D. Su, P. Song, W. Xing, W. Xu, Y. Wang, Z. Jiang, G. Sun, High performance platinum single atom electrocatalyst for oxygen reduction reaction. *Nat. Commun.* **8**, 15938 (2017).
78. J. Liu, M. Jiao, B. Mei, Y. Tong, Y. Li, M. Ruan, P. Song, G. Sun, L. Jiang, Y. Wang, Z. Jiang, L. Gu, Z. Zhou, W. Xu, Carbon-supported divacancy-anchored platinum single-atom electrocatalysts with superhigh Pt utilization for the oxygen reduction reaction. *Angew. Chem. Int. Ed.* **58**, 1163–1167 (2019).
79. S. Li, J. Liu, Z. Yin, P. Ren, L. Lin, Y. Gong, C. Yang, X. Zheng, R. Cao, S. Yao, Y. Deng, X. Liu, L. Gu, W. Zhou, J. Zhu, X. Wen, B. Xu, D. Ma, Impact of coordination environment on atomically dispersed Pt catalyst for oxygen reduction reaction. *ACS Catal.* **10**, 907–913 (2019).
80. E. Luo, H. Zhang, X. Wang, L. Gao, L. Gong, T. Zhao, Z. Jin, J. Ge, Z. Jiang, C. Liu, W. Xing, Single-atom Cr–N_4 sites designed for durable oxygen reduction catalysis in acid media. *Angew. Chem. Int. Ed.* **58**, 12469–12475 (2019).
81. M. Xiao, J. Zhu, G. Li, N. Li, S. Li, Z. P. Cano, L. Ma, P. Cui, P. Xu, G. Jiang, H. Jin, S. Wang, T. Wu, J. Lu, A. Yu, D. Su, Z. Chen, A single-atom iridium heterogeneous catalyst in oxygen reduction reaction. *Angew. Chem. Int. Ed.* **58**, 9640–9645 (2019).
82. X. Wan, X. Liu, Y. Li, R. Yu, L. Zheng, W. Yan, H. Wang, M. Xu, J. Shui, Fe-N-C electrocatalyst with dense active sites and efficient mass transport for high-performance proton exchange membrane fuel cells. *Nat. Catal.* **2**, 259–268 (2019).
83. F. Li, G.-F. Han, H.-J. Noh, S.-J. Kim, Y. Lu, H. Y. Jeong, Z. Fu, J.-B. Baek, Boosting oxygen reduction catalysis with abundant copper single atom active sites. *Energ. Environ. Sci.* **11**, 2263–2269 (2018).
84. L. Jiao, G. Wan, R. Zhang, H. Zhou, S.-H. Yu, H.-L. Jiang, From metal-organic frameworks to single-atom Fe implanted N-doped porous carbons: Efficient oxygen reduction in both alkaline and acidic media. *Angew. Chem. Int. Ed.* **57**, 8525–8529 (2018).

85. Y. Pan, S. Liu, K. Sun, X. Chen, B. Wang, K. Wu, X. Cao, W.-C. Cheong, R. Shen, A. Han, Z. Chen, L. Zheng, J. Luo, Y. Lin, Y. Liu, D. Wang, Q. Peng, Q. Zhang, C. Chen, Y. Li, A bimetallic Zn/Fe polyphthalocyanine-derived single-atom Fe-N_4 catalytic site: A superior trifunctional catalyst for overall water splitting and Zn-air batteries. *Angew. Chem. Int. Ed.* **57**, 8614–8618 (2018).
86. H. Zhang, W. Zhou, T. Chen, B. Y. Guan, Z. Li, X. W. Lou, A modular strategy for decorating isolated cobalt atoms into multichannel carbon matrix for electrocatalytic oxygen reduction. *Energ. Environ. Sci.* **11**, 1980–1984 (2018).
87. K. Jiang, S. Back, A. J. Akey, C. Xia, Y. Hu, W. Liang, D. Schaak, E. Stavitski, J. K. Nørskov, S. Siahrostami, H. Wang, Highly selective oxygen reduction to hydrogen peroxide on transition metal single atom coordination. *Nat. Commun.* **10**, 3997 (2019).
88. H. B. Tao, J. Zhang, J. Chen, L. Zhang, Y. Xu, J. G. Chen, B. Liu, Revealing energetics of surface oxygen redox from kinetic fingerprint in oxygen electrocatalysis. *J. Am. Chem. Soc.* **141**, 13803–13811 (2019).
89. L. Yang, D. Cheng, H. Xu, X. Zeng, X. Wan, J. Shui, Z. Xiang, D. Cao, Unveiling the high-activity origin of single-atom iron catalysts for oxygen reduction reaction. *Proc. Natl. Acad. Sci. U.S.A.* **115**, 6626–6631 (2018).
90. J. Zhang, M. Zhang, Y. Zeng, J. Chen, L. Qiu, H. Zhou, C. Sun, Y. Yu, C. Zhu, Z. Zhu, Single Fe atom on hierarchically porous S, N-codoped nanocarbon derived from porphyra enable boosted oxygen catalysis for rechargeable Zn-air batteries. *Small* **15**, e1900307 (2019).
91. C. Zhu, Q. Shi, B. Z. Xu, S. Fu, G. Wan, C. Yang, S. Yao, J. Song, H. Zhou, D. Du, S. P. Beckman, D. Su, Y. Lin, Hierarchically porous M-N-C (M = Co and Fe) single-atom electrocatalysts with robust MN_x active moieties enable enhanced ORR performance. *Adv. Energy Mater.* **8**, 1801956 (2018).
92. D. Wang, C. Ao, X. Liu, S. Fang, Y. Lin, W. Liu, W. Zhang, X. Zheng, L. Zhang, T. Yao, Coordination-engineered Cu–N_x single-site catalyst for enhancing oxygen reduction reaction. *ACS Appl. Energy Mater.* **2**, 6497–6504 (2019).
93. X. Zhao, X. Liu, B. Huang, P. Wang, Y. Pei, Hydroxyl group modification improves the electrocatalytic ORR and OER activity of graphene supported single and bi-metal atomic catalysts (Ni, Co, and Fe). *J. Mater. Chem. A* **7**, 24583–24593 (2019).
94. Y. Wang, Y.-J. Tang, K. Zhou, Self-adjusting activity induced by intrinsic reaction intermediate in Fe–N–C single-atom catalysts. *J. Am. Chem. Soc.* **141**, 14115–14119 (2019).
95. M. A. Hunter, J. M. T. A. Fischer, Q. H. Yuan, M. Hankel, D. J. Searles, Evaluating the catalytic efficiency of paired, single-atom catalysts for the oxygen reduction reaction. *ACS Catal.* **9**, 7660–7667 (2019).
96. M. Xiao, Y. Chen, J. Zhu, H. Zhang, X. Zhao, L. Gao, X. Wang, J. Zhao, J. Ge, Z. Jiang, S. Chen, C. Liu, W. Xing, Climbing the apex of the ORR volcano plot via binuclear site construction: Electronic and geometric engineering. *J. Am. Chem. Soc.* **141**, 17763–17770 (2019).
97. H. Sun, M. Wang, X. Du, Y. Jiao, S. Liu, T. Qian, Y. Yan, C. Liu, M. Liao, Q. Zhang, L. Meng, L. Gu, J. Xiong, C. Yan, Modulating the d-band center of boron doped single-atom sites to boost the oxygen reduction reaction. *J. Mater. Chem. A* **7**, 20952–20957 (2019).
98. S. Yang, Y. Yu, M. Dou, Z. Zhang, L. Dai, F. Wang, Two-dimensional conjugated aromatic networks as high-site-density and single-atom electrocatalysts for the oxygen reduction reaction. *Angew. Chem. Int. Ed.* **58**, 14724–14730 (2019).
99. Y. Yao, S. Hu, W. Chen, Z.-Q. Huang, W. Wei, T. Yao, R. Liu, K. Zang, X. Wang, G. Wu, W. Yuan, T. Yuan, B. Zhu, W. Liu, Z. Li, D. He, Z. Xue, Y. Wang, X. Zheng, J. Dong, C.-R. Chang, Y. Chen, X. Hong, J. Luo, S. Wei, W.-X. Li, P. Strasser, Y. Wu, Y. Li, Engineering the electronic structure of single atom Ru sites via compressive strain boosts acidic water oxidation electrocatalysis. *Nat. Catal.* **2**, 304–313 (2019).
100. X. Xu, H. Xu, D. Cheng, Design of high-performance MoS_2 edge supported single-metal atom bifunctional catalysts for overall water splitting via a simple equation. *Nanoscale* **11**, 20228–20237 (2019).
101. P. Li, M. Wang, X. Duan, L. Zheng, X. Cheng, Y. Zhang, Y. Kuang, Y. Li, Q. Ma, Z. Feng, W. Liu, X. Sun, Boosting oxygen evolution of single-atomic ruthenium through electronic coupling with cobalt-iron layered double hydroxides. *Nat. Commun.* **10**, 1711 (2019).
102. J. Yan, L. Kong, Y. Ji, J. White, Y. Li, J. Zhang, P. An, S. Liu, S.-T. Lee, T. Ma, Single atom tungsten doped ultrathin α-$Ni(OH)_2$ for enhanced electrocatalytic water oxidation. *Nat. Commun.* **10**, 2149 (2019).
103. W.-H. Lai, L.-F. Zhang, W.-B. Hua, S. Indris, Z.-C. Yan, Z. Hu, B. Zhang, Y. Liu, L. Wang, M. Liu, R. Liu, Y.-X. Wang, J.-Z. Wang, Z. Hu, H.-K. Liu, S.-L. Chou, S.-X. Dou, General π-electron-assisted strategy for Ir, Pt, Ru, Pd, Fe, Ni single-atom electrocatalysts with bifunctional active sites for highly efficient water splitting. *Angew. Chem. Int. Ed.* **58**, 11868–11873 (2019).
104. C. Cai, S. Han, Q. Wang, M. Gu, Direct observation of yolk-shell transforming to gold single atoms and clusters with superior oxygen evolution reaction efficiency. *ACS Nano* **13**, 8865–8871 (2019).
105. H. Zhang, Y. Liu, T. Chen, J. Zhang, J. Zhang, X. W. Lou, Unveiling the activity origin of electrocatalytic oxygen evolution over isolated Ni atoms supported on a N-doped carbon matrix. *Adv. Mater.* **31**, e1904548 (2019).
106. L. Cao, Q. Luo, J. Chen, L. Wang, Y. Lin, H. Wang, X. Liu, X. Shen, W. Zhang, W. Liu, Z. Qi, Z. Jiang, J. Yang, T. Yao, Dynamic oxygen adsorption on single-atomic Ruthenium catalyst with high performance for acidic oxygen evolution reaction. *Nat. Commun.* **10**, 4849 (2019).
107. X. Han, X. Ling, D. Yu, D. Xie, L. Li, S. Peng, C. Zhong, N. Zhao, Y. Deng, W. Hu, Atomically dispersed binary Co-Ni sites in nitrogen-doped hollow carbon nanocubes for reversible oxygen reduction and evolution. *Adv. Mater.* **31**, e1905622 (2019).
108. Y. Lei, Y. Wang, Y. Liu, C. Song, Q. Li, D. Wang, Y. Li, Realizing the atomic active center for hydrogen evolution electrocatalysts. *Angew. Chem. Int. Ed.* 10.1002/ange.201914647, (2020).
109. H. Liu, X. Peng, X. Liu, Single-atom catalysts for the hydrogen evolution reaction. *ChemElectroChem* **5**, 2963–2974 (2018).
110. M. Zhou, S. Bao, A. J. Bard, Probing size and substrate effects on the hydrogen evolution reaction by single isolated Pt atoms, atomic clusters, and nanoparticles. *J. Am. Chem. Soc.* **141**, 7327–7332 (2019).
111. L. Ji, P. Yan, C. Zhu, C. Ma, W. Wu, C. Wei, Y. Shen, S. Chu, J. Wang, Y. Du, J. Chen, X. Yang, Q. Xu, One-pot synthesis of porous 1T-phase MoS_2 integrated with single-atom Cu doping for enhancing electrocatalytic hydrogen evolution reaction. *Appl. Catal. B* **251**, 87–93 (2019).
112. D. Wang, Q. Li, C. Han, Z. Xing, X. Yang, Single-atom ruthenium based catalyst for enhanced hydrogen evolution. *Appl Catal B* **249**, 91–97 (2019).
113. H. Zhang, L. Yu, T. Chen, W. Zhou, X. W. Lou, Surface modulation of hierarchical MoS_2 nanosheets by Ni single atoms for enhanced electrocatalytic hydrogen evolution. *Adv. Funct. Mater.* **28**, 1807086 (2018).
114. Q. Wang, Z. L. Zhao, S. Dong, D. He, M. J. Lawrence, S. Han, C. Cai, S. Xiang, P. Rodriguez, B. Xiang, Z. Wang, Y. Liang, M. Gu, Design of active nickel single-atom decorated MoS_2 as a pH-universal catalyst for hydrogen evolution reaction. *Nano Energy* **53**, 458–467 (2018).
115. J. Zhang, X. Xu, L. Yang, D. Cheng, D. Cao, Single-atom Ru doping induced phase transition of MoS_2 and S vacancy for hydrogen evolution reaction. *Small Methods* **3**, 1900653 (2019).
116. T. S. Zeleke, M.-C. Tsai, M. A. Weret, C.-J. Huang, M. K. Birhanu, T.-C. Liu, C.-P. Huang, Y.-L. Soo, Y.-W. Yang, W.-N. Su, B.-J. Hwang, Immobilized single molecular molybdenum disulfide on carbonized polyacrylonitrile for hydrogen evolution reaction. *ACS Nano* **13**, 6720–6729 (2019).
117. K. Qi, X. Cui, L. Gu, S. Yu, X. Fan, M. Luo, S. Xu, N. Li, L. Zheng, Q. Zhang, J. Ma, Y. Gong, F. Lv, K. Wang, H. Huang, W. Zhang, S. Guo, W. Zheng, P. Liu, Single-atom cobalt array bound to distorted 1T MoS_2 with ensemble effect for hydrogen evolution catalysis. *Nat. Commun.* **10**, 5231 (2019).
118. X. Lv, W. Wei, P. Zhao, D. Er, B. Huang, Y. Dai, T. Jacob, Oxygen-terminated BiXenes and derived single atom catalysts for the hydrogen evolution reaction. *J. Catal.* **378**, 97–103 (2019).
119. D. A. Kuznetsov, Z. Chen, P. V. Kumar, A. Tsoukalou, A. Kierzkowska, P. M. Abdala, O. V. Safonova, A. Fedorov, C. R. Müller, Single site cobalt substitution in 2D molybdenum carbide (MXene) enhances catalytic activity in the hydrogen evolution reaction. *J. Am. Chem. Soc.* **141**, 17809–17816 (2019).
120. V. Ramalingam, P. Varadhan, H.-C. Fu, H. Kim, D. Zhang, S. Chen, L. Song, D. Ma, Y. Wang, H. N. Alshareef, J.-H. He, Heteroatom-mediated interactions between ruthenium single atoms and an MXene support for efficient hydrogen evolution. *Adv. Mater.* **31**, e1903841 (2019).
121. Y. Zhao, T. Ling, S. Chen, B. Jin, A. Vasileff, Y. Jiao, L. Song, J. Luo, S.-Z. Qiao, Non-metal single-iodine-atom electrocatalysts for the hydrogen evolution reaction. *Angew. Chem. Int. Ed.* **58**, 12252–12257 (2019).
122. C.-H. Chen, D. Wu, Z. Li, R. Zhang, C.-G. Kuai, X.-R. Zhao, C.-K. Dong, S.-Z. Qiao, H. Liu, X.-W. Du, Ruthenium-based single-atom alloy with high electrocatalytic activity for hydrogen evolution. *Adv. Energy Mater.* **9**, 1803913 (2019).
123. J. Yang, B. Chen, X. Liu, W. Liu, Z. Li, J. Dong, W. Chen, W. Yan, T. Yao, X. Duan, Y. Wu, Y. Li, Efficient and robust hydrogen evolution: Phosphorus nitride imide nanotubes as supports for anchoring single ruthenium sites. *Angew. Chem. Int. Ed.* **57**, 9495–9500 (2018).
124. K. Jiang, B. Liu, M. Luo, S. Ning, M. Peng, Y. Zhao, Y.-R. Lu, T.-S. Chan, F. M. F. de Groot, Y. Tan, Single platinum atoms embedded in nanoporous cobalt selenide as electrocatalyst for accelerating hydrogen evolution reaction. *Nat. Commun.* **10**, 1743 (2019).
125. L. Zhang, R. Si, H. Liu, N. Chen, Q. Wang, K. Adair, Z. Wang, J. Chen, Z. Song, J. Li, M. N. Banis, R. Li, T.-K. Sham, M. Gu, L.-M. Liu, G. A. Botton, X. Sun, Atomic layer deposited Pt-Ru dual-metal dimers and identifying their active sites for hydrogen evolution reaction. *Nat. Commun.* **10**, 4936 (2019).
126. X. P. Gao, Y. Zhou, Z. Cheng, Y. Tan, S. Liu, Z. Shen, Doping sp-hybridized B atoms in graphyne supported single cobalt atoms for hydrogen evolution electrocatalysis. *Int. J. Hydrogen Energy* **44**, 27421–27428 (2019).

127. Y. Zhao, D. Ma, J. Zhang, Z. Lu, Y. Wang, Transition metal embedded C_3N monolayers as promising catalysts for the hydrogen evolution reaction. *Phys. Chem. Chem. Phys.* **21**, 20432–20441 (2019).
128. J. N. Tiwari, A. M. Harzandi, M. Ha, S. Sultan, C. W. Myung, H. J. Park, D. Y. Kim, P. Thangavel, A. N. Singh, P. Sharma, S. S. Chandrasekaran, F. Salehnia, J.-W. Jang, H. S. Shin, Z. Lee, K. S. Kim, High-performance hydrogen evolution by Ru single atoms and nitrided-Ru nanoparticles implanted on N-doped graphitic sheet. *Adv. Energy Mater.* **9**, 1900931 (2019).
129. X. Gao, Y. Zhou, Y. Tan, B. Yang, Z. Cheng, Z. Shen, Single Mo atoms supported on N-doped carbon with N/C edge-site for enhanced electrochemical hydrogen evolution. *Int. J. Hydrogen Energy* **44**, 14861–14868 (2019).
130. T. W. He, C. M. Zhang, A. Du, Single-atom supported on graphene grain boundary as an efficient electrocatalyst for hydrogen evolution reaction. *Chem. Eng. Sci.* **194**, 58–63 (2019).
131. J. N. Tiwari, S. Sultan, C. W. Myung, T. Yoon, N. Li, M. Ha, A. M. Harzandi, H. J. Park, D. Y. Kim, S. S. Chandrasekaran, W. G. Lee, V. Vij, H. Kang, T. J. Shin, H. S. Shin, G. Lee, Z. Lee, K. S. Kim, Multicomponent electrocatalyst with ultralow Pt loading and high hydrogen evolution activity. *Nat. Energy* **3**, 773–782 (2018).
132. W. Chen, J. Pei, C.-T. He, J. Wan, H. Ren, Y. Wang, J. Dong, K. Wu, W.-C. Cheong, J. Mao, X. Zheng, W. Yan, Z. Zhuang, C. Chen, Q. Peng, D. Wang, Y. Li, Single tungsten atoms supported on MOF-derived N-doped carbon for robust electrochemical hydrogen evolution. *Adv. Mater.* **30**, e1800396 (2018).
133. X.-P. Yin, H.-J. Wang, S.-F. Tang, X.-L. Lu, M. Shu, R. Si, T.-B. Lu, Engineering the coordination environment of single-atom platinum anchored on graphdiyne for optimizing electrocatalytic hydrogen evolution. *Angew. Chem. Int. Ed.* **57**, 9382–9386 (2018).
134. D. Liu, X. Li, S. Chen, H. Yan, C. Wang, C. Wu, Y. A. Haleem, S. Duan, J. Lu, B. Ge, P. M. Ajayan, Y. Luo, J. Jiang, L. Song, Atomically dispersed platinum supported on curved carbon supports for efficient electrocatalytic hydrogen evolution. *Nat. Energy* **4**, 512–518 (2019).
135. Y. Xue, B. Huang, Y. Yi, Y. Guo, Z. Zuo, Y. Li, Z. Jia, H. Liu, Y. Li, Anchoring zero valence single atoms of nickel and iron on graphdiyne for hydrogen evolution. *Nat. Commun.* **9**, 1460 (2018).
136. L. Cao, Q. Luo, W. Liu, Y. Lin, X. Liu, Y. Cao, W. Zhang, Y. Wu, J. Yang, T. Yao, S. Wei, Identification of single-atom active sites in carbon-based cobalt catalysts during electrocatalytic hydrogen evolution. *Nat. Catal.* **2**, 134–141 (2019).
137. D. Gao, R. M. Arán-Ais, H. S. Jeon, B. R. Cuenya, Rational catalyst and electrolyte design for CO_2 electroreduction towards multicarbon products. *Nat. Catal.* **2**, 198–210 (2019).
138. C. Costentin, S. Drouet, M. Robert, J.-M. Savéant, A local proton source enhances CO_2 electroreduction to CO by a molecular Fe catalyst. *Science* **338**, 90–94 (2012).
139. E. Zhang, T. Wang, K. Yu, J. Liu, W. Chen, A. Li, H. Rong, R. Lin, S. Ji, X. Zheng, Y. Wang, L. Zheng, C. Chen, D. Wang, J. Zhang, Y. Li, Bismuth single atoms resulting from transformation of metal-organic frameworks and their use as electrocatalysts for CO_2 reduction. *J. Am. Chem. Soc.* **141**, 16569–16573 (2019).
140. X. Su, X.-F. Yang, Y. Huang, B. Liu, T. Zhang, Single-atom catalysis toward efficient CO_2 conversion to CO and formate products. *Acc. Chem. Res.* **52**, 656–664 (2018).
141. G. Wan, G. Zhang, X.-M. Lin, Toward efficient carbon and water cycles: Emerging opportunities with single-site catalysts made of 3d transition metals. *Adv. Mater.* **32**, e1905548 (2019).
142. L. Gong, D. Zhang, C.-Y. Lin, Y. Zhu, Y. Shen, J. Zhang, X. Han, L. Zhang, Z. Xia, Catalytic mechanisms and design principles for single-atom catalysts in highly efficient CO_2 conversion. *Adv. Energy Mater.* **9**, 1902625 (2019).
143. H. Yang, L. Shang, Q. Zhang, R. Shi, G. I. N. Waterhouse, L. Gu, T. Zhang, A universal ligand mediated method for large scale synthesis of transition metal single atom catalysts. *Nat. Commun.* **10**, 4585 (2019).
144. X. Qin, S. Zhu, F. Xiao, L. Zhang, M. Shao, Active sites on heterogeneous single-iron-atom electrocatalysts in CO_2 reduction reaction. *ACS Energy Lett.* **4**, 1778–1783 (2019).
145. Y. Chen, L. Zou, H. Liu, C. Chen, Q. Wang, M. Gu, B. Yang, Z. Zou, J. Fang, H. Yang, Fe and N Co-doped porous carbon nanospheres with high density of active sites for efficient CO_2 electroreduction. *J. Phys. Chem. C* **123**, 16651–16659 (2019).
146. T. N. Huan, N. Ranjbar, G. Rousse, M. Sougrati, A. Zitolo, V. Mougel, F. Jaouen, M. Fontecave, Electrochemical reduction of CO_2 catalyzed by Fe-N-C materials: A structure–selectivity study. *ACS Catal.* **7**, 1520–1525 (2017).
147. J. Gu, C.-S. Hsu, L. Bai, H. M. Chen, X. Hu, Atomically dispersed Fe^{3+} sites catalyze efficient CO_2 electroreduction to CO. *Science* **364**, 1091–1094 (2019).
148. C. Zhao, X. Dai, T. Yao, W. Chen, X. Wang, J. Wang, J. Yang, S. Wei, Y. Wu, Y. Li, Ionic exchange of metal organic frameworks to access single nickel sites for efficient electroreduction of CO_2. *J. Am. Chem. Soc.* **139**, 8078–8081 (2017).
149. Q. Fan, P. Hou, C. Choi, T.-S. Wu, S. Hong, F. Li, Y.-L. Soo, P. Kang, Y. Jung, Z. Sun, Activation of Ni particles into single Ni–N atoms for efficient electrochemical reduction of CO_2. *Adv. Energy Mater.* **10**, 1903068 (2020).
150. S. Ma, P. Su, W. Huang, S. P. Jiang, S. Bai, J. Liu, Atomic Ni species anchored N-doped carbon hollow spheres as nanoreactors for efficient electrochemical CO_2 reduction. *ChemCatChem* **11**, 6092–6098 (2019).
151. K. Mou, Z. Chen, X. Zhang, M. Jiao, X. Zhang, X. Ge, W. Zhang, L. Liu, Highly efficient electroreduction of CO_2 on nickel single-atom catalysts: Atom trapping and nitrogen anchoring. *Small* **15**, e1903668 (2019).
152. D. M. Koshy, S. Chen, D. U. Lee, M. B. Stevens, A. M. Abdellah, S. M. Dull, G. Chen, D. Nordlund, A. Gallo, C. Hahn, D. C. Higgins, Z. Bao, T. F. Jaramillo, Understanding the origin of highly selective CO_2 electroreduction to CO on Ni,N-doped carbon catalysts. *Angew. Chem. Int. Ed.* **59**, 4043–4050 (2020).
153. Y.-N. Gong, L. Jiao, Y. Qian, C.-Y. Pan, L. Zheng, X. Cai, B. Liu, S.-H. Yu, H.-L. Jiang, Regulating the coordination environment of MOF-templated single-atom nickel electrocatalysts for boosting CO_2 reduction. *Angew. Chem. Int. Ed.* **59**, 2705–2709 (2020).
154. X. Rong, H.-J. Wang, X.-L. Lu, R. Si, T.-B. Lu, Controlled synthesis of a vacancy-defect single-atom catalyst for boosting CO_2 electroreduction. *Angew. Chem. Int. Ed.* **59**, 1961–1965 (2020).
155. T. Zheng, K. Jiang, N. Ta, Y. Hu, J. Zeng, J. Liu, H. Wang, Large-scale and highly selective CO_2 electrocatalytic reduction on nickel single-atom catalyst. *Joule* **3**, 265–278 (2019).
156. C. Zhao, Y. Wang, Z. Li, W. Chen, Q. Xu, D. He, D. Xi, Q. Zhang, T. Yuan, Y. Qu, J. Yang, F. Zhou, Z. Yang, X. Wang, J. Wang, J. Luo, Y. Li, H. Duan, Y. Wu, Y. Li, Solid-diffusion synthesis of single-atom catalysts directly from bulk metal for efficient CO_2 reduction. *Joule* **3**, 584–594 (2019).
157. B.-W. Zhang, Y. Jiao, D.-L. Chao, C. Ye, Y.-X. Wang, K. Davey, H.-K. Liu, S.-X. Dou, S.-Z. Qiao, Targeted synergy between adjacent Co atoms on graphene oxide as an efficient new electrocatalyst for Li–CO_2 batteries. *Adv. Funct. Mater.* **29**, 1904206 (2019).
158. H. Zhou, X. Zou, X. Wu, X. Yang, J. Li, Coordination engineering in cobalt-nitrogen-functionalized materials for CO_2 reduction. *J. Phys. Chem. Lett.* **10**, 6551–6557 (2019).
159. Y. Wu, Z. Jiang, X. Lu, Y. Liang, H. Wang, Domino electroreduction of CO_2 to methanol on a molecular catalyst. *Nature* **575**, 639–642 (2019).
160. J. Li, P. Pršlja, T. Shinagawa, A. J. M. Fernández, F. Krumeich, K. Artyushkova, P. Atanassov, A. Zitolo, Y. Zhou, R. García-Muelas, N. López, J. Pérez-Ramírez, F. Jaouen, Volcano trend in electrocatalytic CO_2 reduction activity over atomically dispersed metal sites on nitrogen-doped carbon. *ACS Catal.* **9**, 10426–10439 (2019).
161. J. Zhao, Z. Chen, J. Zhao, F. Liu, Single Mn atom as a promising electrocatalyst for CO reduction to C_2H_5OH and C_3H_6: A computational study. *Appl. Surf. Sci.* **498**, 143868 (2019).
162. S. Dou, J. Song, S. Xi, Y. Du, J. Wang, Z.-F. Huang, Z. J. Xu, X. Wang, Boosting electrochemical CO_2 reduction on metal–organic frameworks via ligand doping. *Angew. Chem.* **131**, 4081–4085 (2019).
163. B. Zhang, J. Zhang, J. Shi, D. Tan, L. Liu, F. Zhang, C. Lu, Z. Su, X. Tan, X. Cheng, B. Han, L. Zheng, J. Zhang, Manganese acting as a high-performance heterogeneous electrocatalyst in carbon dioxide reduction. *Nat. Commun.* **10**, 2980 (2019).
164. W. Zheng, J. Yang, H. Chen, Y. Hou, Q. Wang, M. Gu, F. He, Y. Xia, Z. Xia, Z. Li, B. Yang, L. Lei, C. Yuan, Q. He, M. Qiu, X. Feng, Atomically defined undercoordinated active sites for highly efficient CO_2 electroreduction. *Adv. Funct. Mater.* **30**, 1907658 (2019).
165. D. Karapinar, N. T. Huan, N. R. Sahraie, J. Li, D. Wakerley, N. Touati, S. Zanna, D. Taverna, L. H. G. Tizei, A. Zitolo, F. Jaouen, V. Mougel, M. Fontecave, Electroreduction of CO_2 on single-site copper-nitrogen-doped carbon material: Selective formation of ethanol and reversible restructuration of the metal sites. *Angew. Chem. Int. Ed.* **58**, 15098–15103 (2019).
166. Z. L. Zhao, G. Lu, Cu-based single-atom catalysts boost electroreduction of CO_2 to CH_3OH: First-principles predictions. *J. Phys. Chem. C* **123**, 4380–4387 (2019).
167. Y. Jiao, Y. Zheng, P. Chen, M. Jaroniec, S.-Z. Qiao, Molecular scaffolding strategy with synergistic active centers to facilitate electrocatalytic CO_2 reduction to hydrocarbon/alcohol. *J. Am. Chem. Soc.* **139**, 18093–18100 (2017).
168. X. Liu, Y. Jiao, Y. Zheng, M. Jaroniec, S.-Z. Qiao, Building up a picture of the electrocatalytic nitrogen reduction activity of transition metal single-atom catalysts. *J. Am. Chem. Soc.* **141**, 9664–9672 (2019).
169. B. Yu, H. Li, J. White, S. Donne, J. Yi, S. Xi, Y. Fu, G. Henkelman, H. Yu, Z. Chen, T. Ma, Tuning the catalytic preference of ruthenium catalysts for nitrogen reduction by atomic dispersion. *Adv. Funct. Mater.* **30**, 1905665 (2020).
170. H. Tao, C. Choi, L.-X. Ding, Z. Jiang, Z. Han, M. Jia, Q. Fan, Y. Gao, H. Wang, A. W. Robertson, S. Hong, Y. Jung, S. Liu, Z. Sun, Nitrogen fixation by Ru single-atom electrocatalytic reduction. *Chem* **5**, 204–214 (2019).
171. Z. G. Geng *et al.*, Achieving a record-high yield rate of 120.9 $\mu g_{NH_3}\, mg_{cat.}^{-1}\, h^{-1}$ for N_2 electrochemical reduction over Ru single-atom catalysts. *Adv. Mater.* **30**, e1803498 (2018).
172. W. Zang, T. Yang, H. Zou, S. Xi, H. Zhang, X. Liu, Z. Kou, Y. Du, Y. P. Feng, L. Shen, L. Duan, J. Wang, S. J. Pennycook, Copper single atoms anchored in porous nitrogen-doped carbon as efficient pH-universal catalysts for the nitrogen reduction reaction. *ACS Catal.* **9**, 10166–10173 (2019).
173. H. R. Guo, L. Li, X. Wang, G. Yao, H. Yu, Z. Tian, B. Li, L. Chen, Theoretical investigation on the single transition-metal atom-decorated defective MoS_2 for electrocatalytic ammonia synthesis. *ACS Appl. Mater. Interfaces* **11**, 36506–36514 (2019).
174. Q. Li, C. Liu, S. Qiu, F. Zhou, L. He, X. Zhang, C. Sun, Exploration of iron borides as electrochemical catalysts for the nitrogen reduction reaction. *J. Mater. Chem. A* **7**, 21507–21513 (2019).
175. Y. Qiu, X. Peng, F. Lü, Y. Mi, L. Zhuo, J. Ren, X. Liu, J. Luo, Single-atom catalysts for the electrocatalytic reduction of nitrogen to ammonia under ambient conditions. *Chem. Asian J.* **14**, 2770–2779 (2019).

176. Y. Wan, J. Xu, R. Lv, Heterogeneous electrocatalysts design for nitrogen reduction reaction under ambient conditions. *Mater. Today* **27**, 69–90 (2019).
177. F. Lü, S. Zhao, R. Guo, J. He, X. Peng, H. Bao, J. Fu, L. Han, G. Qi, J. Luo, X. Tang, X. Liu, Nitrogen-coordinated single Fe sites for efficient electrocatalytic N-2 fixation in neutral media. *Nano Energy* **61**, 420–427 (2019).
178. W. Zhao, L. Zhang, Q. Luo, Z. Hu, W. Zhang, S. Smith, J. Yang, Single $Mo_1(Cr_1)$ atom on nitrogen-doped graphene enables highly selective electroreduction of nitrogen into ammonia. *ACS Catal.* **9**, 3419–3425 (2019).
179. T. He, S. K. Matta, A. Du, Single tungsten atom supported on N-doped graphyne as a high-performance electrocatalyst for nitrogen fixation under ambient conditions. *Phys. Chem. Chem. Phys.* **21**, 1546–1551 (2019).
180. S. Zheng, S. Li, Z. Mei, Z. Hu, M. Chu, J. Liu, X. Chen, F. Pan, Electrochemical nitrogen reduction reaction performance of single-boron catalysts tuned by MXene substrates. *J. Phys. Chem. Lett.* **10**, 6984–6989 (2019).
181. P. Ou, X. Zhou, F. Meng, C. Chen, Y. Chen, J. Song, Single molybdenum center supported on N-doped black phosphorus as an efficient electrocatalyst for nitrogen fixation. *Nanoscale* **11**, 13600–13611 (2019).
182. H.-R. Zhu, Y.-L. Hu, S.-H. Wei, D.-Y. Huai, Single-metal atom anchored on boron monolayer (β_{12}) as an electrocatalyst for nitrogen reduction into ammonia at ambient conditions: A first-principles study. *J. Phys. Chem. C* **123**, 4274–4281 (2019).
183. C. Liu, Q. Li, C. Wu, J. Zhang, Y. Jin, D. R. MacFarlane, C. Sun, Single-boron catalysts for nitrogen reduction reaction. *J. Am. Chem. Soc.* **141**, 2884–2888 (2019).

Acknowledgments
Funding: This work was supported by the National Key R&D Program of China (2016YFA0202804), the Strategic Priority Research Program of the Chinese Academy of Sciences (XDB36030200), the National Natural Science Foundation of China (grant no. 21925803), the Singapore Ministry of Education Academic Research Fund (AcRF) Tier 1: RG115/17 and RG 115/18, and Tier 2: MOE2016-T2-2-004, and Singapore Energy Center (SgEC) SgEC-Core2019-15. **Author contributions:** X.L., L.L., X.R., and J.G. cowrote the manuscript. X.L., B.L., and Y.H. edited the manuscript. **Competing interests:** The authors declare that they have no competing interests. **Data and materials availability:** All data needed to evaluate the conclusions in the paper are present in the paper. Additional data related to this paper may be requested from the authors.

Submitted 11 March 2020
Accepted 7 August 2020
Published 23 September 2020
10.1126/sciadv.abb6833

Citation: X. Li, L. Liu, X. Ren, J. Gao, Y. Huang, B. Liu, Microenvironment modulating of single-atom catalysts and the roles in electrochemical energy conversion. *Sci. Adv.* **6**, eabb6833 (2020).